POLITECNICO DI MILANO

School of Industrial and Information Engineering

Department of Mechanical Engineering

BLADE LOADS ANALYSIS OF A SCALED WIND TURBINE MODEL.

Master Thesis Dissertation of:

Rahul Bharath Krishni Gurumoorthy

Student ID: 918139

Supervisor:
Prof.Sara Muggiasca

Co-supervisor:
Eng. Alessandro Fontanella

Academic Year – 2020 – 2021

Page intentionally left blank.

Abstract

This thesis is about the process of interpretation and simulation of the measured load data and analyzing it with transformed data. Starting with the literature survey about blade aerodynamic forces measurement and sensor techniques for precise measuring. Followed by obtaining the wind turbine model parameters, simulation is done using the aerodynamic test results. FAST simulation tool and MATLAB software were utilized for the analysis respectively .

Abstract (Italian)

Questa tesi riguarda il processo di interpretazione e simulazione dei dati di carico misurati e l'analisi con dati trasformati. A partire dall'indagine bibliografica sulla misurazione delle forze aerodinamiche della pala e sulle tecniche dei sensori per una misurazione precisa. Seguita dall'ottenimento dei parametri del modello della turbina eolica, la simulazione viene eseguita utilizzando i risultati dei test aerodinamici. Lo strumento di simulazione FAST e il software MATLAB sono stati utilizzati rispettivamente per l'analisi.

Acknowledgement

As a Master of science student at Politecnico di Milano, I have gained a lot as I grew up professionally and an opportunity to know the diversity of cultures and colleagues and overcome many challenges. Like any compelling adventure, the university studies are not a path that is tackled alone; I would like to express my gratitude to a number of persons who have influenced the outcome of my master's studies and thesis in various ways.

First and foremost, I would want to thank my supervisor, Prof. Sara Muggiasca, for the chance. I gratefully acknowledge my co-supervisor Eng.Alessandro Fontanella for his continuous support of my research. Without their continuous support, it would have not been possible to complete this study.

I would like to take this occasion to offer my heartfelt thanks and respectful regards to the academics and teaching personnel at Politecnico di Milano's Mechanical Engineering department., for sharing their knowledge during attending the courses and gave me untiring help during my study.

Finally, I must express my very profound gratitude to my Family and Friends for all the love support throughout my life.

Table of contents

List of figures

LIST OF TABLES

List of abbreviations

CFRP	Carbon Fiber Reinforced Plastic
DOF	Degrees of Freedom
DTU	Danmarks Tekniske Universitet
FAST	Fatigue, Aerodynamics, Structure and Turbulence
FE	Finite Element
FEA	Finite Element Analysis
FOWT	Floating Offshore Wind Turbine
HAWT	Horizontal Axis Wind Turbine
IEC	International Electrotechnical Commission
NOEL	Natural Ocean Engineering Laboratory
NREL	National Renewable Energy Laboratory
RELM	Element Location from Rotor Axis of Rotation
RPM	Round Per Minute
RWT	Reference Wind Turbine
VAWT	Vertical Axis Wind Turbine
WT	Wind Turbine

1 INTRODUCTION

1.1 Wind as an energy source:

In recent times, wind energy emerged as one of the most important and promising sources of renewable energy, which demands better means of maintaining system reliability. Wind power has emerged as an alternative to conventional power generation. It has established itself as a major source of non-polluting, inexhaustible renewable energy. Through technology innovations and economies of scale, the global wind power market has nearly quadrupled in size over the past decade and managed itself as one of the most cost efficient and manageable power sources across the world.

Thanks to technology breakthroughs and economies of scale, the global wind power sector has nearly doubled in size in the previous decade, establishing itself as one of the most cost-effective and reliable power sources on the planet

In 2020, record growth was driven by an increase in installations in China and the United States, the world's two largest wind power markets, which together installed about 75% of new installations and account for more than half of the world's total wind power capacity in 2020. [2]

Today, 743 GW of wind generating capacity exists around the world, helping to avoid roughly 1.1 billion tonnes of CO2 — the equivalent of South America's yearly carbon emissions.[2]

However, as the clean energy technology with the greatest decarbonization potential per MW, the report shows that current wind power deployment rates will not be enough to achieve carbon neutrality by the middle of this century, and policymakers must act quickly to scale up wind power at the required rate.

To keep global warming well below 2°c over the pre-industrial levels, the world needs to install an average of 180 GW of new wind energy per year, and from 2030 onwards, it will need to install up to 280 GW annually to stay on track to attain net zero by 2050.

[2]

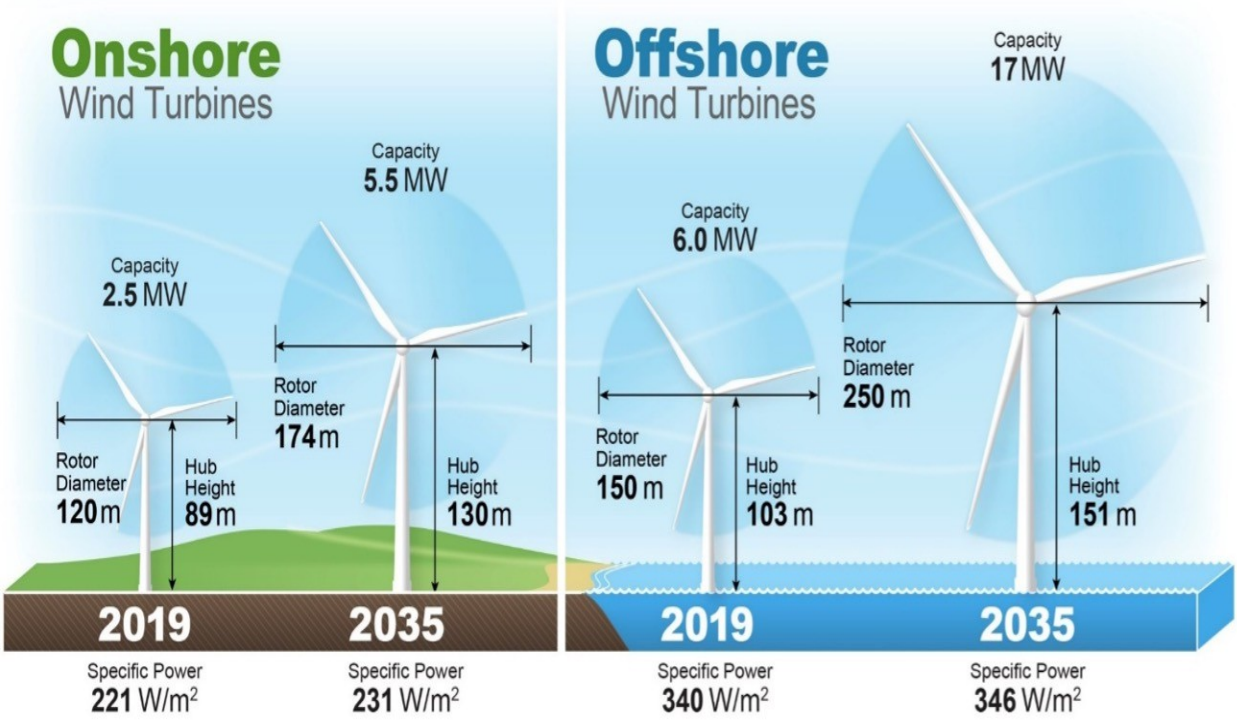

Figure 1.1 -Wind Turbine capacity forecast[4]

1.2 Floating offshore wind turbines :

Offshore wind farms are projected to account for a large fraction of total wind energy output and may even become a significant contributor to total electricity production in some nations, as wind power continues to increase rapidly around the world. Because of the close proximity of high-quality wind resources to coastal energy loads, offshore wind turbines have the potential to make a significant contributor to global energy production..

The higher loading reduces the reliability of offshore turbines, hence the ability to minimise loads is critical for offshore wind turbines, as it allows for increased reliability.

The global pipeline for floating offshore wind energy will have grown by more than thrice by 2020. Since the "2019 Offshore Wind Technologies Data Update," the global floating offshore wind pipeline for 2020 has grown by 18,866 MW, from 7,663 MW to 26,529 MW.. This increase might be attributable to the fact that various projects, particularly in Asian markets, are starting the planning phase in 2020. [3]

Figure 1.2 Offshore Wind Turbine [1]

1.3 Objective

The prime objective of this thesis is to run the simulation of blade forces in FAST environment and compare the results with the other simulation tool such as MATLAB. The analysis involves that the measured loads at Root blade matched with the transformed measured values of tower top loads. Hence, the motive is to estimate the forces at main blade by using tower top load values.

1.4 Synopsis

This thesis is organized as follows:

Chapter 2 Explains about the state of art and critical review of scaling process of the wind turbine model and its features.

Chapter 3 Describes about the configuration of the FAST module.

Chapter 4 Describes about the Load measurement analysis.

Chapter 5 Describes about the results of the analysis

2 State of the art

Literature review outline:

A detailed literature survey on scaling process, Thruster's load sensing and main blade Load measurement techniques has been carried out.

i. The measurement of loads using load cell techniques has been analyzed through various articles.
ii. The scaling process of the wind turbine model with their conditions and previous outcomes are studied and the brief is discussed further.
iii. The load measurement techniques in a propeller thruster is analyzed from the article [43].The underwater conditions, spindle forces, thrust, torque variations are studied to know the arrangement and parameters that could be helpful for our analysis motive.
iv. Finally, the Individual pitch control of blades were studied to know about the pitch demand and its effectiveness in maintaining the thrust and torque. So, maintaining a good measurement of the loads on the blade.

The detailed study on the experimental conditions and setup of our model is discussed further:

2.1 Scaling Process of the model .

The scale factor is defined as the ratio between a general DTU 10 MW reference wind turbine parameter and the corresponding wind tunnel model parameter.

$$\lambda = (\mathbf{P}_{reference} / \mathbf{P}_{model})$$

The dimensional analysis technique is fundamental in model design for wind tunnel. A series of non-dimensional groups are usually considered, the most used are the Reynolds number, Froude Number, Strouhal Number, Cauchy number, etc. Usually the length scale, λL, is defined from simple considerations about the wind tunnel dimension, then one of the non-dimensional groups is selected to be kept constant from full scale to model scale. The choice is made considering which are the most important parameters that influence tests results.

The blade design aims at matching as close as possible the scaled values of the turbine aerodynamic thrust and torque. The reference model we used for the scaling process is DTU 10MW RWT and its parameters are given in the following table:

Parameter	DTU 10MW RWT
Wind Regime	IEC Class 1A
Rotor Orientation	Clockwise rotation - Upwind
VS Control	Variable Speed
Pitch Control	Collective Pitch
Cut-in wind speed	4 m/s
Cut-out wind speed	25 m/s
Rated wind speed	11.4 m/s
Rated power	10 MW
Number of blades	3
Rotor Diameter	178.3 m
Hub Diameter	5.6 m
Hub Height	119.0 m
Gearbox	Medium Speed Multiple Stage
Minimum Rotor Speed	6.0 RPM
Maximum Rotor Speed	9.6 RPM
Maximum Generator Speed	480.0 RPM
Gearbox Ratio	50:1
Maximum Tip Speed	90.0 m/s
Hub Overhang	7.1 m
Shaft Tilt Angle	5.0°
Rotor Precone Angle	−2.5°
Blade Prebend	3.332 m
Rotor Mass	227 962 kg
Nacelle Mass	446 036 kg
Tower Mass	628 442 kg

Table 2.1 DTU 10 MW reference wind turbine model parameters

Main turbine parts classification:

About Figure 2.1 three different functional groups can be identified:

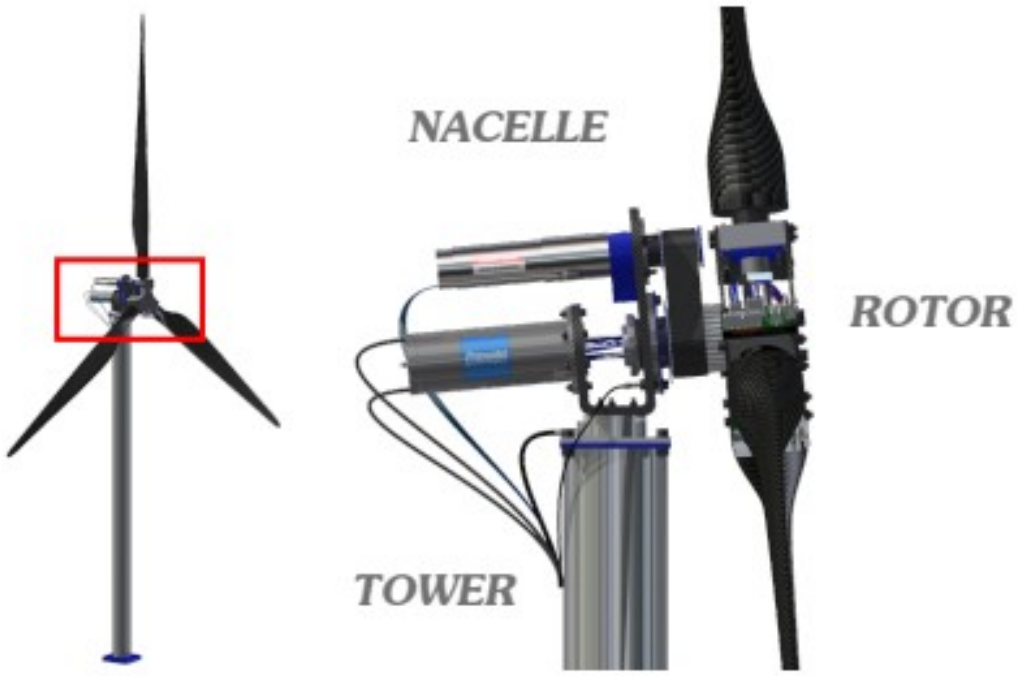

Figure 2.1 Scale model wind turbine assembly [23]

• **Nacelle**: the nacelle represents the connection between the tower and the rotor; the characteristic elements of this group are the main shaft motor, which is misaligned with respect to the main shaft. The transmission is realized by means of a toothed belt.

It is important to mention the presence of the slip ring which guarantees the connection for the IPC motors, in which the power supply and digital/analog signals input/output.

• **Rotor** : two subgroups can be identified, the hub and the blades. Two different pitch control mechanisms were designed, a manual one, adopted during the first wind tunnel session for the deliverable and the motor-drive IPC system.

• **Tower top**: the functional element of the tower is a 6-axes balance which is placed between the nacelle and a connection flange on the top of the tower to measure the overall rotor forces.

2.1.1 Nacelle

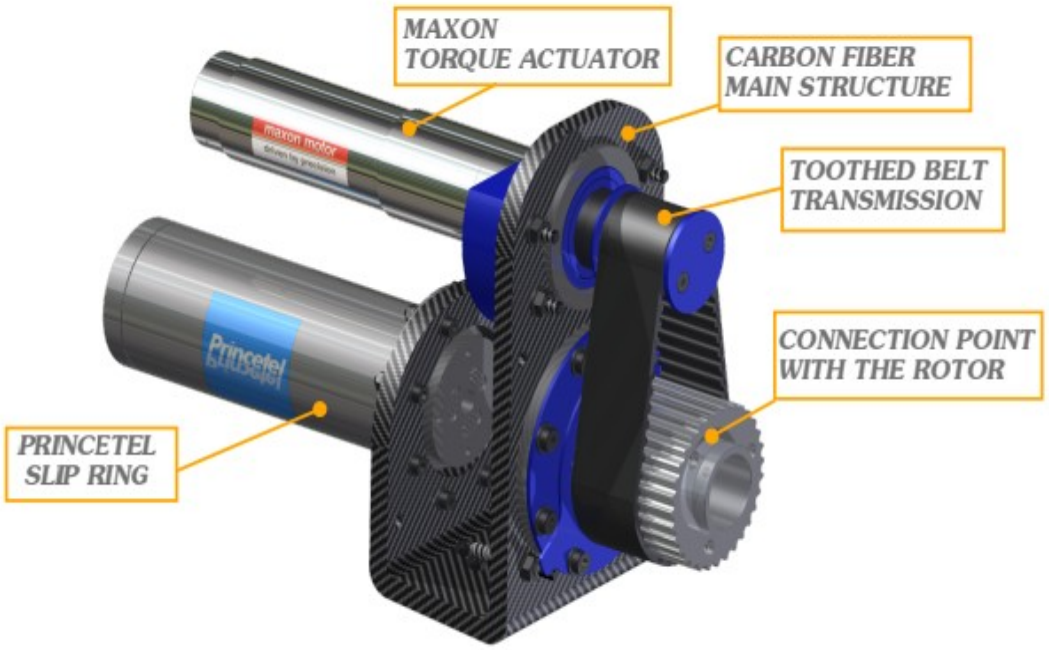

(a) Nacelle assembly.

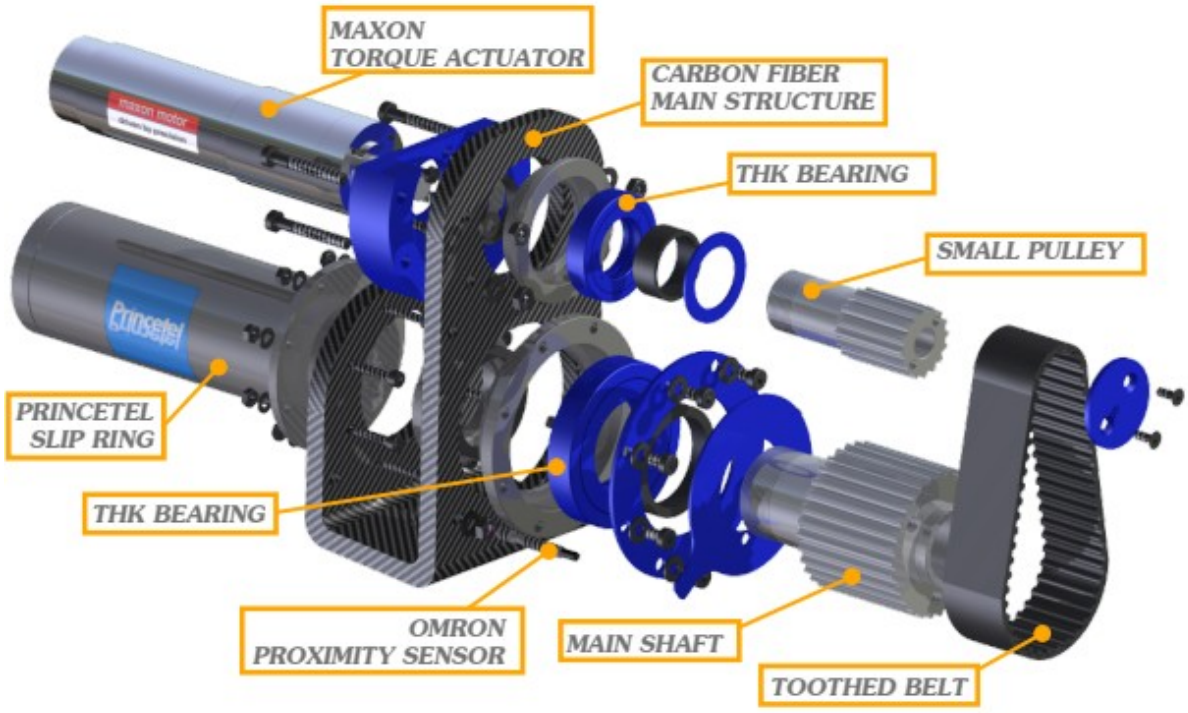

(b) Nacelle exploded view.

Figure 2.1.1 Nacelle CAD model.

The nacelle, represented in Figure 2.1.1 , is characterized by a ”U-shaped” structure made of high modulus carbon fiber structure, whose aim is to guarantee the correct positioning of the main shaft motor, the slip ring device, the main shaft, and the rotor tilt angle. In addition to it, the under surface of this element is directly connected to 6 axis balances. The frontal surface is inclined in order to guarantee the prescribed 5-degree tilt angle for the main shaft. The high stiffness of the carbon fiber allows to have a very thin structure and to reduce the overall weight.

The main shaft and the primary motor were placed on two different axes to let the electrical wires from the slip ring to reach the drives of the IPC motors; this necessitated the hollowing of the main shaft. Another unique aspect is the mechanism that supports both the main shaft and the pulley that connects to the primary motor; in fact, using traditional ball bearings to bear bending moments would necessitate two of these parts for each axis, resulting in a larger structure and more weight.

Cross-roller bearings appeared to be the greatest option, as they conserve space and can withstand extremely high bending moments while weighing the same as a single ball bearing.

The external cup of the cross-roller bearings is held in two aluminum casings that are directly attached to the carbon fiber frame. While the upper bearing exterior cup is attached to the aluminum case, the bottom one is held in place by an aluminum flange that is screwed to the aluminum case. As previously stated, motion is transmitted from the main motor to the main shaft through a toothed belt with a transmission ratio of 2. The idea of using a gear-to-gear coupling has been discarded because it would have led to an excessive increment of mass.

In general, finding a commercial solution that fits these criteria is not difficult, but the mass constraints severely limited the number of alternatives. A brushless DC motor with a transmission ratio of 21: 1 and a magnetic encoder with a resolution of 500 [1/ rev] proved to be the optimum choice. A hard plastic support piece (ABS) created with a 3D printer secures the main motor to the carbon fibre construction.

2.1.2 Rotor

As mentioned before the rotor can be further divided into the hub and the three blades. A view of the rotor is reported in Figure 2.1.2.The structural supports of the roots of the blades are given by a two-carbon fiber triangular plates and by three aluminum blocks, whose aim is to keep the distance between the two plates, as well as to hold the two versions of the pitch regulation mechanisms. To make the hub even stiffer three carbon fiber hollowed spacers are placed between the plates. As can be noticed, the plate which is in contact with the main shaft is characterized by a

hole that allows to mount the rotor on the main shaft with a high precision centering between the rotor axis and the main shaft itself.

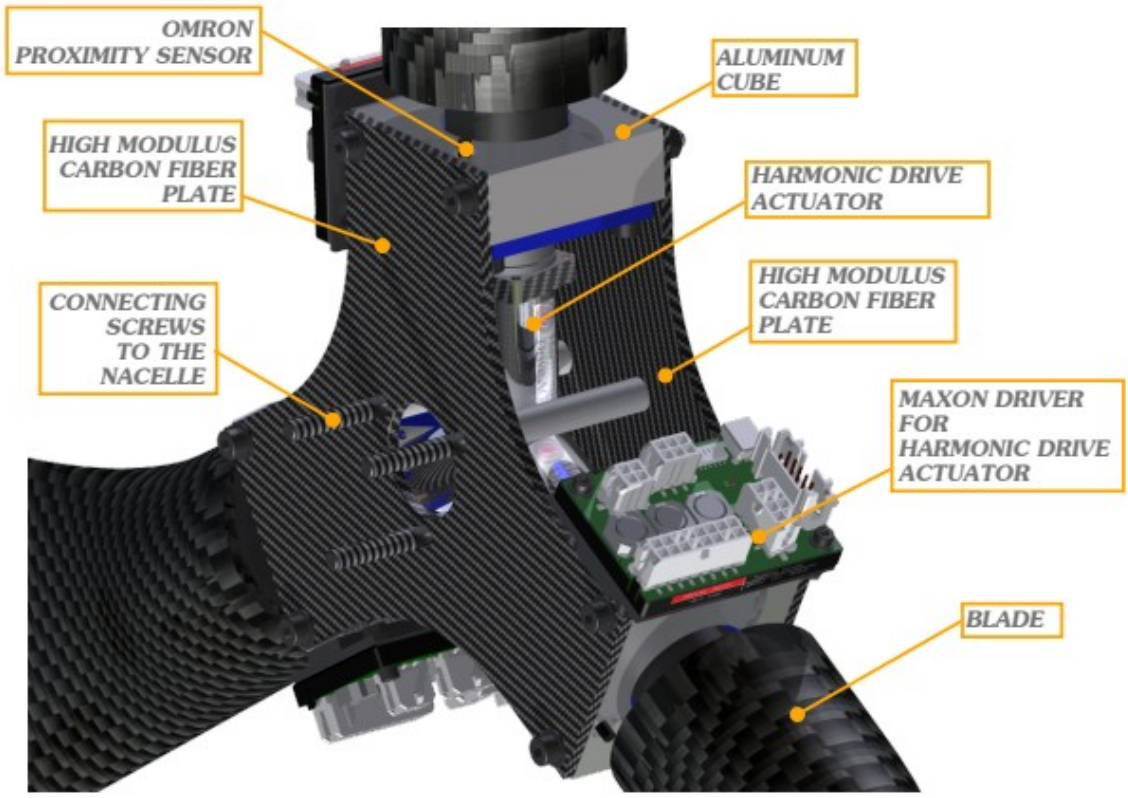

(a) Rotor assembly.

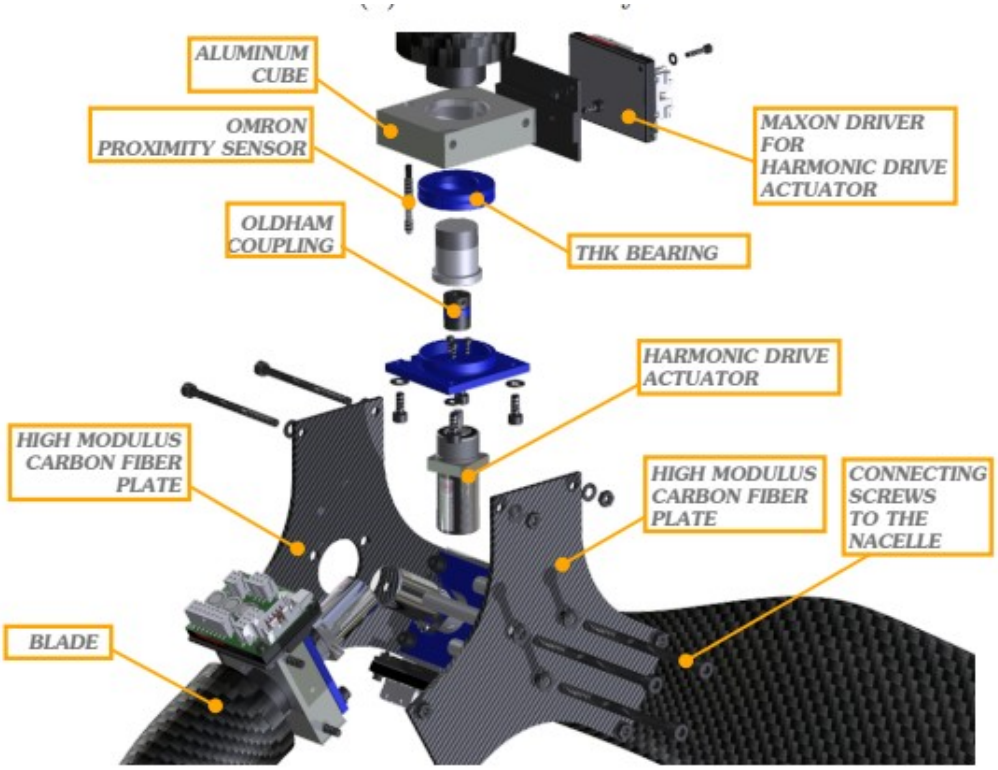

(b) Rotor exploded view.

Figure 2.1.2 Rotor CAD model.

Furthermore, this kind of coupling provides the correct transmission of the shear stresses from the rotor to the main shaft and then to the cross-roller bearing. The fixing between hub and main shaft is achieved by means of three long screws that go through the plates and the spacers to end up into three threaded holes located on the frontal surface of the main shaft. It is also necessary to eliminate the possibility of vibration events invalidating the results in this application. It is thus of fundamental importance to ensure that the hub structure is sufficiently

2.1.3 Tower top

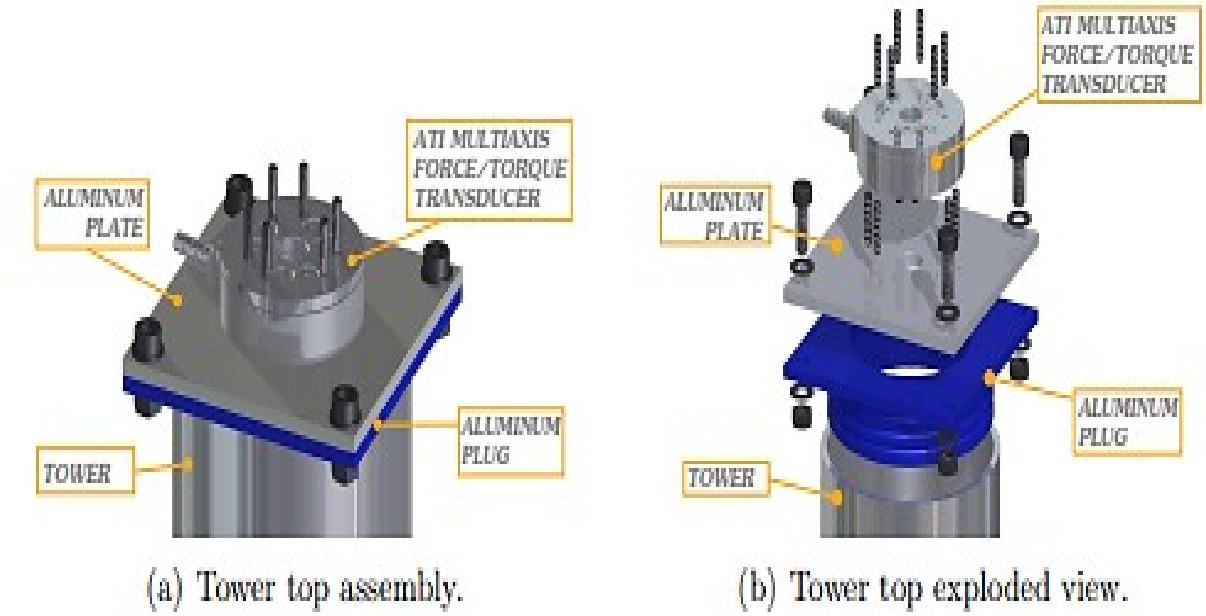

Figure 2.1.3: Tower top CAD model.

Figure 2.1.3 shows the assembled and exploded view of the tower top. The principal element is the 6-axes balance whose top surface is directly connected to the nacelle carbon fiber structure whereas the bottom surface is fixed to an aluminum plate which is fixed to an aluminum plug glued to the tower. Furthermore, it can measure torques up to ±5 Nm about all the axes. During all the design process a parametric approach has been adopted, especially for the aero-elastic version of the model., also allowing a direct view of the effect on the overall mass due to any modification and to compare them with the requirements.

Assembly	DTU 10MW RTW $[kg]$	DTU down-scaled $[kg]$	PoliMi 10MW WTM $[kg]$
Nacelle	446036	1.057	1.788
Rotor (blade+hub)	227962	0.540	1.255
Single blade	41716	0.099	0.210

Table 3. Mass goals and results.

Table 3 shows the final masses of the functional groups compared to the downscaled DTU 10MW wind turbine.

2.2 Wind tunnel test setup

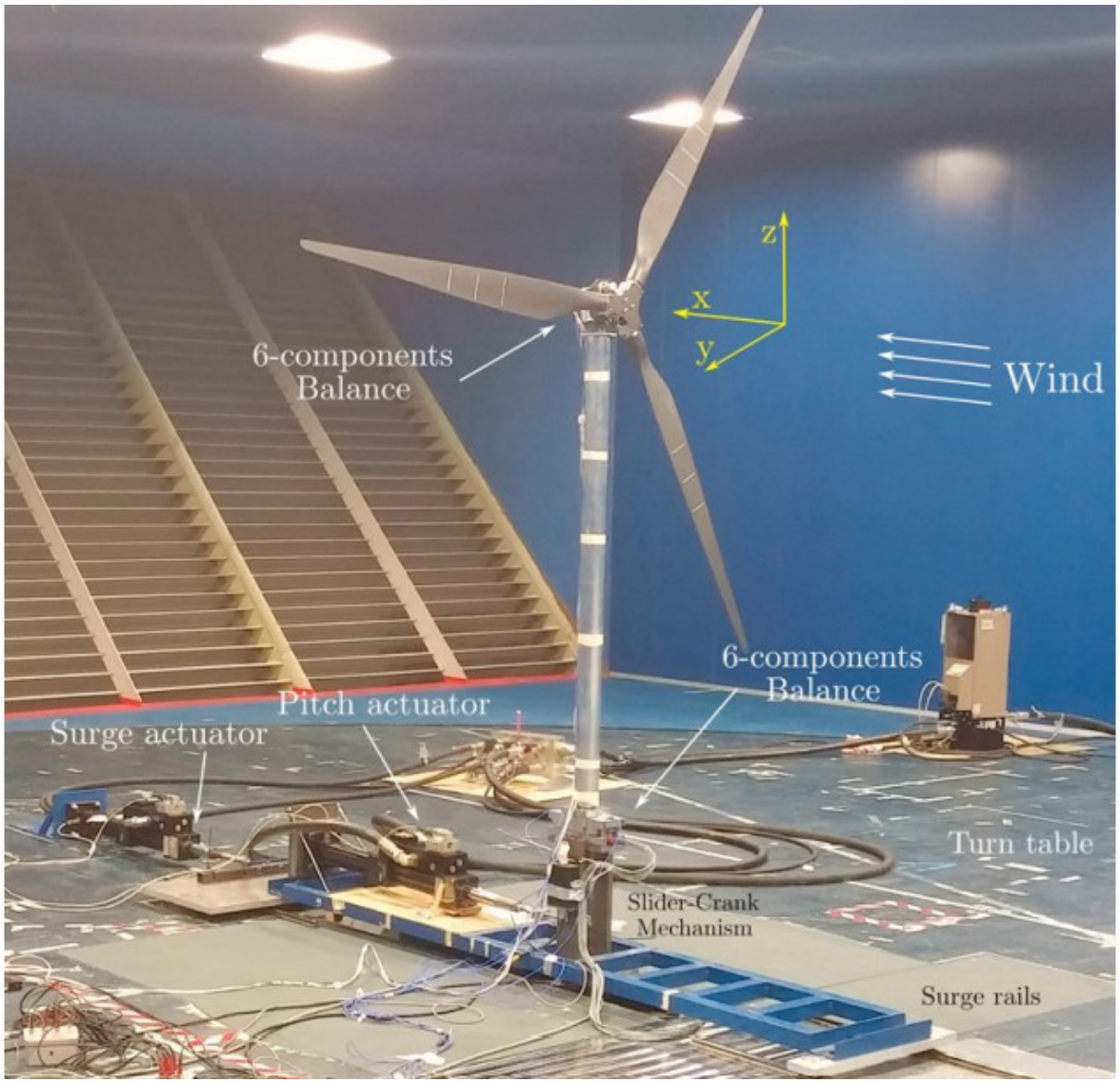

Figure 2.2.1 Wind tunnel setup

Figure 2.2.1 shows the setup to carry out the aerodynamics tests of the scaled wind turbine model in the wind tunnel. [10]

During the wind tunnel tests, a series of wind turbine dynamic conditions were tested, over three different wind tunnel speeds: rated wind speed at 3.67 m/s, below the rated at 2.33 m/s and one above the rated at 5.33 m/s.

These three conditions were chosen as representative of all the possible wind condition normally encountered by the turbine in operation, in aerodynamic sense. Either the rotational speed or blade pitch were kept fixed at the corresponding nominal values during the tests.

In this work, we are simulating using 2 wind flow conditions either steady or turbulent. The nacelle position is changed, and the load data are generated for the various conditions. The figure 2.2.2 shows the nacelle positions to the wind direction.

To make sure the scaled model is ready for further analysis, the important test is to match the thrust of the reference wind turbine, the curve is matched during the test and experiment is carried on further.

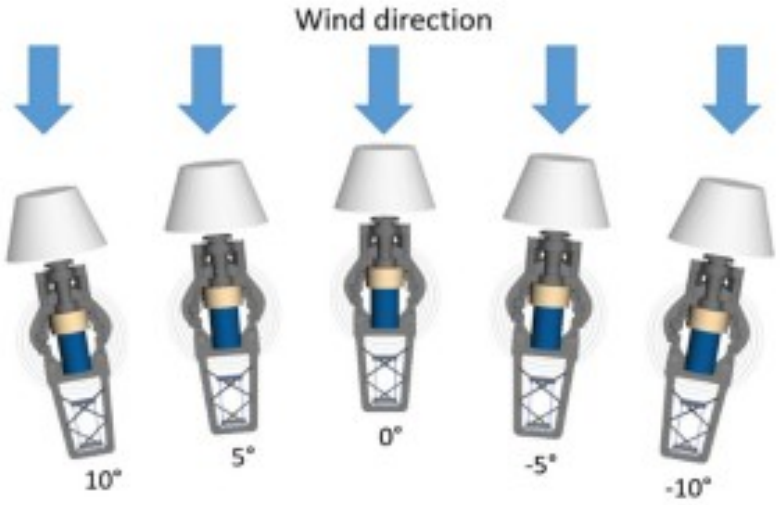

Figure 2.2.2 Nacelle position to the wind direction[44]

2.3 Individual Pitch control of blades:

Individual pitch control, in which the pitch of each blade is modified individually in response to recorded loads, can significantly reduce fatigue loading on a wind turbine. The asymmetrical out-of-plane rotor load is assessed, and for each blade, an additional pitch action (dominated by the rotor's rotational frequency) is computed to reduce the burden. This results in the near-elimination of the main once-per-revolution ('1P') peak in the rotating components' out-of-plane load spectra, and fatigue loads can be decreased by 20%–40%.

The load reduction is also transferred to the nacelle and tower, but only the low-frequency loads are removed, resulting in a load reduction of only a few percent at most, because the fatigue on the fixed components is dominated by the peak at the blade passing frequency ('3P' for a three-bladed turbine), which is largely unaffected by individual pitch control action.

This shows how a simple modification to the individual pitch control algorithm can minimize the dominant load peak on fixed components, resulting in considerable fatigue load reductions over the whole structure.[24]

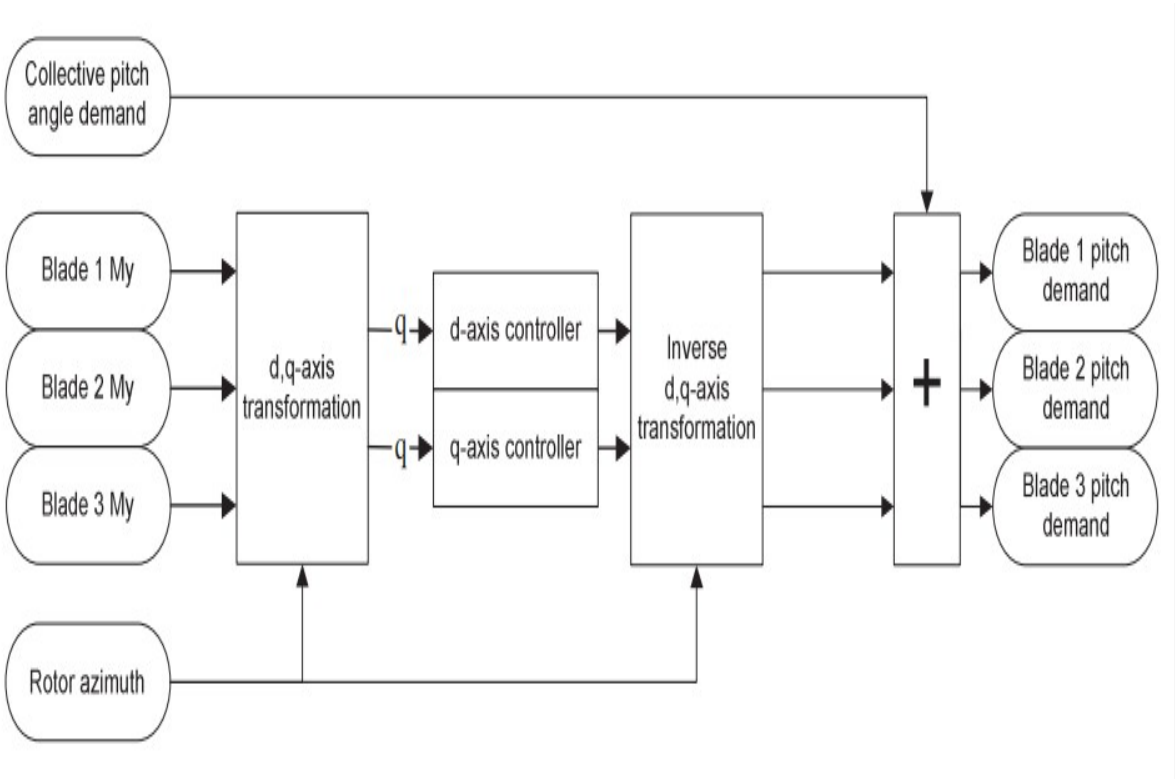

Figure 2.3.1 Individual Pitch control scheme

Individual pitch control as we know it today has been around for a long time and has its origins in helicopter technology. In recent years, there has been renewed interest in this technique since wind turbines have grown in ratio to the scale of turbulent structures in the wind, increasing the importance of asymmetrical loadings.

There is also a raising desire to decrease structural costs by reducing the loads by intelligent controls, which has the potential to be a cheaper idea than building very strong structures to tolerate the high potential loads. Finally, modern sensor technologies, such as fiber optics, can now provide the high level of reliability required by this application at an affordable price. Few approaches were undergone by different researchers with the details of the current technique, which predicts fatigue load reductions of 20 percent to 30 percent at the blade roots and 30 percent to 40 percent at the hub.

Figure 2.3.1 demonstrates how out-of-plane bending moment signals (typically generated from flap wise and edgewise signals resolved through the pitch angle) are

transformed into two orthogonal d- and q-axes (which can be regarded of as the horizontal and vertical axes) using an unique transformation.

A controller for each axis generates a pitch demand for that axis, and the reverse transformation converts the two d- and q-axis pitch demands into pitch demand increments for each blade. To get a total pitch demand for each blade, these are added together with the collective pitch demand (which governs torque and thrust and thus rotational speed, tower vibration, and so on). The two axes can be controlled independently,a two-input, two-output technique can also be employed to control both axes at the same time, but the added complexity does not appear to provide any meaningful benefit.

Previous research has also shown that the d- and q-axis loading signals can be derived from measurement devices situated on the rotor hub, main shaft, or even non-rotating sections of the construction. Although there are practical advantages and disadvantages to different sensor placements, they are all equivalent as inputs to the individual pitch controller. The collective pitch control is normally triggered by the observed generator speed, but it can also be triggered by nacelle acceleration.

One potential benefit of using load sensors in the blade roots is that, in addition to feeding individual pitch control, the signals can be used to estimate rotor torque and thrust, which can then be included in the collective pitch control algorithm to improve the quality of the collective pitch control loop performance. Other feasible load sensor positions could also be employed, but they may be less handy in this case. Blade root sensors would also be much easier to calibrate using the blade self-weight: the controller might include an automatic method to check the calibrations during periods of low wind speed (below cut in).

In theory, the filter may be built not only to remove the 3P response, but also to minimise the 3P component of fixed frame loads by adjusting the amplitude and phase of the compensator's 3P response. The feedforward filter is introduced as an alternate approach. This new filter picks out the 3P load component and modifies the phase to create an additional contribution to the individual pitch demands, lowering the 3P load component.

The d- or q-axis pitch demand now consists of two parts: a low-frequency component from the PI controller, which adjusts the asymmetrical load to the appropriate value (usually zero), and a mainly 3P component from the feedforward filter with zero mean.

Because tweaking the feedforward filter is not easy, a limited numerical optimization technique in the frequency domain has been devised specifically for this purpose. Limits can be set on the PI controller output, which has the effect of restricting the magnitude of the 1P individual pitch fluctuations at each blade. To phase out the individual pitch control action below rated, for example, a limit determined as a function of generator power or torque can be employed.

The limit can also be used to ensure that the final pitch position requirement does not exceed any physical pitch position constraints. The feedforward filter can also be subjected to the limit schedule. In theory, when the turbine needs to yaw, a non-zero set-point for the PI controller working on the axis representing the yaw moment might be utilised, causing the individual pitch action to generate a yawing moment, assisting (or possibly replacing) the yaw motor in yawing the turbine.

The yaw misalignment and up flow can also be estimated using the d- and q-axis pitch demands. This might be used instead of the wind vane as an input to the yaw control algorithm with appropriate lowpass filtering.

2.3.1 Results of IPC study

Figure 2.3.1.1 shows frequency spectra of the blade root out-of-plane (My) bending moment, the rotating hub My load (Mz is very similar) and the yaw bearing yaw moment Mz representing the fixed frame loads (the nodding moment My is very similar). The spectrum of the total pitch rate for one blade is also shown, the basic individual pitch control removes the dominant 1P load peak on the rotating components (at about 0·3 Hz in this case).

On the fixed components this means that the low frequencies are removed, leaving the fatigue-dominating 3P (blade passing frequency) peak almost unchanged—this is the peak at about 0·9 Hz. This is achieved by additional pitch action which is almost entirely at 1P. The spectra for the runs including the new feedforward term show that the basic 1P action is still the same, but some additional pitch action is introduced at frequencies above 3P which has the effect of reducing the 3P peak in the fixed frame loads. There is also a further slight reduction in the rotating loads.

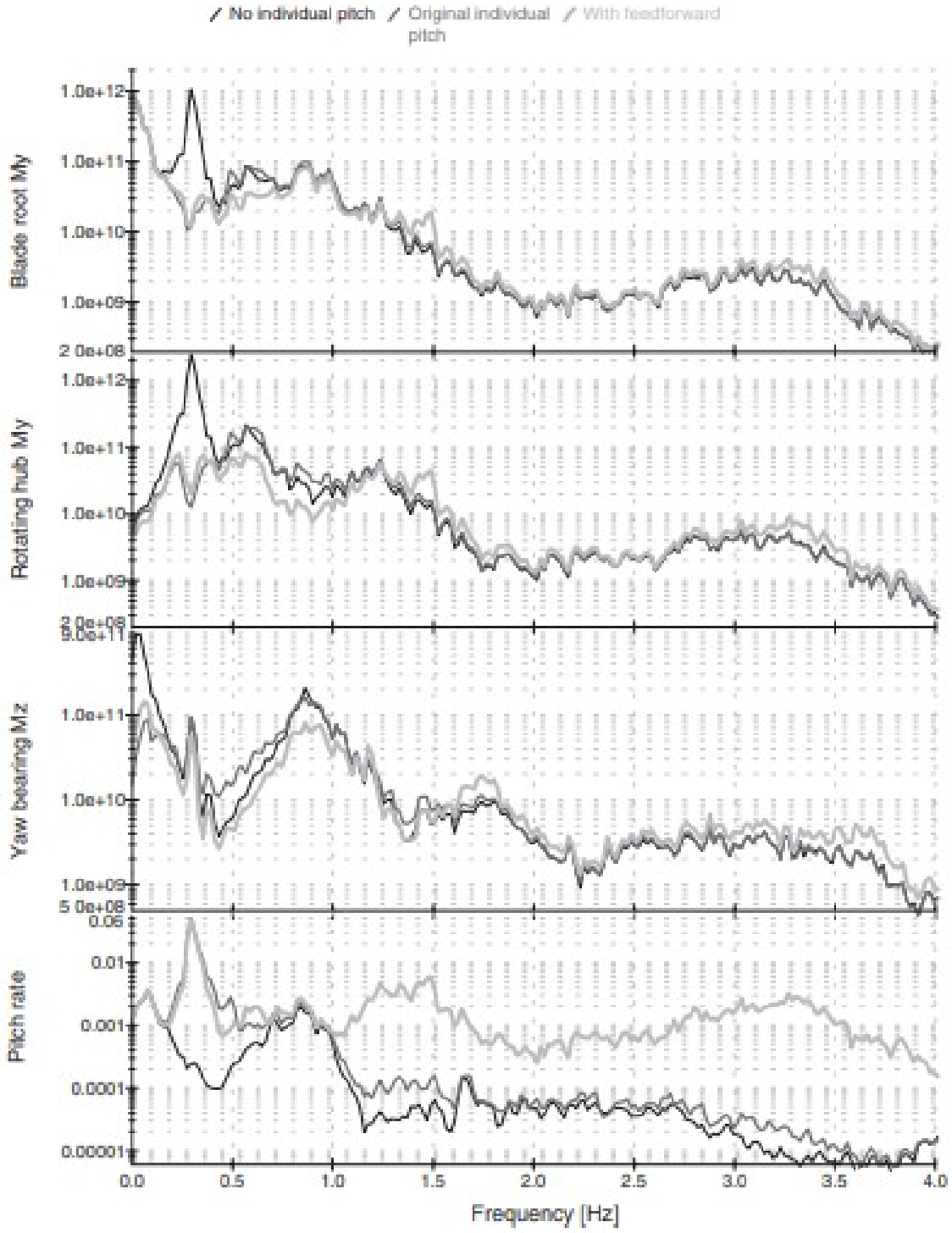

Figure 2.3.1.1 Spectrum of Pitch rate and main turbine loads

To sum it up, A development has been made to the previously mentioned individual pitch control approach. Additional large load reductions, notably for fixed frame loads, are accomplished by introducing a specific feedforward term in parallel with the PI controllers for the d- and q-axes, at the expense of a further rise in pitch activity.

3 Configuration of FAST Module parameters

Before configuring the FAST module conditions let see about different wind type that affects analysis and measurement of each load and ease of the understanding of different parameters.

3.1 Wind Types

The power is produced from a wind turbine is by the interaction between the airfoils of each rotor blade and the wind. Air flowing over the blades' airfoil generates aerodynamic lift and drag forces. The resulting aerodynamic loads on the blades and the turbine can be subdivided into three categories.

1. Steady aerodynamic forces generated by the mean wind speed.

2. Periodic aerodynamic forces generated by wind shear, rotor rotation, off-axis winds, and tower shadow.

3. Randomly fluctuating aerodynamic forces induced by gusts, turbulence, and dynamic effects.

the steady aerodynamic loads are important for long-term power production estimations. Periodic loads mainly are associated with resonance issues and govern the design of the system's natural frequencies. Lastly, fluctuating loads due to turbulence affect the fatigue lifetime and gusts—which are short-term effects—dominate the ultimate loads.

The required strength of most of the system's components usually is governed by fatigue loads. AeroDyn—the aerodynamics module of FAST—models these aerodynamic effects that cause the loads described above. Nevertheless, to calculate the aerodynamics in acceptable computation time, substantial simplifications are made to account for the various effects. AeroDyn uses the blade element momentum (BEM) theory to calculate the aerodynamic forces and moments on the blades.

This theory captures the primary features of the air flow in and around wind turbines: The induced velocities due to power production and the rotation of the expanding turbine wake downwind. Empirical corrections are required to overcome the simplicity of the BEM theory, which assumes of uniform induction on radial annuli and steady two- dimensional aerodynamics, but neglects, for example, the interdependence of the airflows at adjacent radial blade sections.

The corrections include the Prandtl tip-loss model to capture the effect of reduced lift at the blade tips. Further losses from the airflow around the rotor hub also are modeled.

A dynamic inflow model based on the generalized dynamic wake (GDW) theory is implemented to consider unsteady, turbulent wind inflow. The airfoil data is augmented to account for some rotational 3D effects and unsteady airfoil

aerodynamics. The effect of turbulent-wake-state that occurs if the rotor strongly decelerates the axial airflow also is considered, as is wake inertia or some 3-D effects such as stall delay.

The dynamics of stalled blades during turbine operation are simulated using a Beddoes-Leishman dynamic stall model. The actual flow field and aerodynamics, however, are more complex and the capabilities of the correction models to account for the various influences that are not captured by simple BEM theory are limited.

3.2 Scaled Model Parameters feed to FAST

DTU 10.0 WTM aerodynamic input properties.

STEADY	StallMod	- Dynamic stall model [BEDDOES or STEADY]
NO_CM NO_CM]	UseCm	- Aerodynamic pitching moment model [USE_CM or
EQUIL	InfModel	- Inflow model [DYNIN or EQUIL]
SWIRL	IndModel	- Induction factor model [NONE or WAKE or SWIRL]
0.005	AToler	- Convergence tolerance for induction factor
PRANDtl	TLModel	- Tip-loss model (for EQUIL only) [PRANdtl, GTECH
PRANDtl	HLModel	- Hub-loss model (for EQUIL only) [PRANdtl,
0	TwrShad	- Tower-shadow velocity deficit (-)
9999.9	ShadHWid	- Tower-shadow half width (m)
9999.9	T_Shad_Refpt	- Tower-shadow reference point (m)
1.225	AirDens	- Air density (kg/m^3)
1.464E-5	KinVisc	- Kinematic air viscosity (m^2/sec)
default bjj: was 0.02479	DTAero	- Time interval for aerodynamic calculations (sec) !
39	NumFoil	- Number of airfoil files used. Files listed below:

Table 3.2.1 Aerodyn Input parameters

```
------- ELASTODYN V1.00.* INDIVIDUAL BLADE INPUT FILE ------------------------
10MW DTU Wind Tunnel Model Blade input file. A. Fontanella
---------------------- BLADE PARAMETERS ---------------------------------------
        27   NBlInpSt    - Number of blade input stations (-)
     0.925   BldFlDmp(1) - Blade flap mode #1 structural damping in percent of critical (%) - WRONG
     1.345   BldFlDmp(2) - Blade flap mode #2 structural damping in percent of critical (%) - WRONG
     0.765   BldEdDmp(1) - Blade edge mode #1 structural damping in percent of critical (%) - WRONG
---------------------- BLADE ADJUSTMENT FACTORS -------------------------------
         1   FlStTunr(1) - Blade flapwise modal stiffness tuner, 1st mode (-)
         1   FlStTunr(2) - Blade flapwise modal stiffness tuner, 2nd mode (-)
    3.2432   AdjBlMs     - Factor to adjust blade mass density. Added to match the experimental blade mass. (-)
    0.6506   AdjFlSt     - Factor to adjust blade flap stiffness. Added to match the experimental first collective flap mode. (-)
         1   AdjEdSt     - Factor to adjust blade edge stiffness (-)
---------------------- DISTRIBUTED BLADE PROPERTIES ---------------------------
BlFract        PitchAxis      StrcTwst       BMassDen       FlpStff        EdgStff
(-)            (-)            (deg)          (kg/m)         (Nm^2)         (Nm^2)
0.0000000e+00  5.0000000e-01  -2.1457254e-01  7.1163228e-02  2.3298206e+03  9.9999999e9



---------------------- BLADE MODE SHAPES ---------------
     0.0644   BldFl1Sh(2) - Flap mode 1, coeff of x^2
     3.4722   BldFl1Sh(3) -            , coeff of x^3
    -5.1286   BldFl1Sh(4) -            , coeff of x^4
     3.8062   BldFl1Sh(5) -            , coeff of x^5
    -1.2142   BldFl1Sh(6) -            , coeff of x^6
    -0.3457   BldFl2Sh(2) - Flap mode 2, coeff of x^2
   -14.2306   BldFl2Sh(3) -            , coeff of x^3
    29.7596   BldFl2Sh(4) -            , coeff of x^4
   -14.9296   BldFl2Sh(5) -            , coeff of x^5
     0.7464   BldFl2Sh(6) -            , coeff of x^6
      1.352   BldEdgSh(2) - Edge mode 1, coeff of x^2
     1.5862   BldEdgSh(3) -            , coeff of x^3
    -6.1184   BldEdgSh(4) -            , coeff of x^4
     6.6006   BldEdgSh(5) -            , coeff of x^5
    -2.4203   BldEdgSh(6) -            , coeff of x^6
```

Figure 3.2.1 Blade Properties

```
------ InflowWind v3.01.* INPUT FILE ------------------------------------------------------------------------
Wind case for Scaled 10 MW DTU.
---------------------------------------------------------------------------------------------------------------
False        Echo          - Echo input data to <RootName>.ech (flag)
        1    WindType      - switch for wind file type (1=steady; 2=uniform; 3=binary TurbSim FF; 4=binary Bladed-style FF; 5=HAWC format; 6=User defined)
        0    PropagationDir - Direction of wind propagation (meteoroligical rotation from aligned with X (positive rotates towards -Y) -- degrees)
        1    NWindVel      - Number of points to output the wind velocity    (0 to 9)
        0    WindVxiList   - List of coordinates in the inertial X direction (m)
        0    WindVyiList   - List of coordinates in the inertial Y direction (m)
      1.6    WindVziList   - List of coordinates in the inertial Z direction (m)
================== Parameters for Steady Wind Conditions [used only for WindType = 1] =======================
      3.8    HWindSpeed    - Horizontal windspeed                           (m/s)
      1.6    RefHt         - Reference height for horizontal wind speed     (m)
        0    PLexp         - Power law exponent                             (-)
================== Parameters for Uniform wind file   [used only for WindType = 2] ============================
"unused"     Filename      - Filename of time series data for uniform wind field.      (-)
               1.6                 RefHt         - Reference height for horizontal wind speed              (m)
      9999.9                 RefLength     - Reference length for linear horizontal and vertical sheer (-)
================== Parameters for Binary TurbSim Full-Field files   [used only for WindType = 3] ==============
"unused"    Filename      - Name of the Full field wind file to use (.bts)
================== Parameters for Binary Bladed-style Full-Field files   [used only for WindType = 4] =========
"unused"    FilenameRoot  - Rootname of the full-field wind file to use (.wnd, .sum)
False       TowerFile     - Have tower file (.twr) (flag)
```

Figure 3.2.2 Wind cases

```
------- ELASTODYN V1.00.* TOWER INPUT FILE -------------------------------------
Scaled 10MW tower data. Correct mass distribution, wrong stiffness. A. F. Sette.
---------------------- TOWER PARAMETERS ----------------------------------------
         11   NTwInpSt     - Number of input stations to specify tower geometry, da portare a 20!
       6.28   TwrFADmp(1) - Tower 1st fore-aft mode structural damping ratio (%)
       6.28   TwrFADmp(2) - Tower 2nd fore-aft mode structural damping ratio (%)
          6.28   TwrSSDmp(1) - Tower 1st side-to-side mode structural damping ratio (%)
       6.28   TwrSSDmp(2) - Tower 2nd side-to-side mode structural damping ratio (%)
---------------------- TOWER ADJUSTMUNT FACTORS --------------------------------
          1   FAStTunr(1) - Tower fore-aft modal stiffness tuner, 1st mode (-)
          1   FAStTunr(2) - Tower fore-aft modal stiffness tuner, 2nd mode (-)
          1   SSStTunr(1) - Tower side-to-side stiffness tuner, 1st mode (-)
          1   SSStTunr(2) - Tower side-to-side stiffness tuner, 2nd mode (-)
          1   AdjTwMa     - Factor to adjust tower mass density (-)
          1   AdjFASt     - Factor to adjust tower fore-aft stiffness (-)
          1   AdjSSSt     - Factor to adjust tower side-to-side stiffness (-)
```

Figure 3.2.3 Tower Data

Finally, the Elastodyn Input Conditions are configured,

```
---------------------- INITIAL CONDITIONS ---------------------------------
         0   OoPDefl     - Initial out-of-plane blade-tip displacement (meters)
                0   IPDefl      - Initial in-plane blade-tip deflection (meters)
            0  BlPitch(1)  - Blade 1 initial pitch (degrees)
            0   BlPitch(2)  - Blade 2 initial pitch (degrees)
            0    BlPitch(3)  - Blade 3 initial pitch (degrees)
         0   TeetDefl    - Initial or fixed teeter angle (degrees) [unused for 3 blades]
         0   Azimuth     - Initial azimuth angle for blade 1 (degrees)
       240   RotSpeed    - Initial or fixed rotor speed (rpm)
         0   NacYaw      - Initial or fixed nacelle-yaw angle (degrees)
         0   TTDspFA     - Initial fore-aft tower-top displacement (meters)
         0   TTDspSS     - Initial side-to-side tower-top displacement (meters)
         0   PtfmSurge   - Initial or fixed horizontal surge translational displacement of platform (meters)
         0   PtfmSway    - Initial or fixed horizontal sway translational displacement of platform (meters)
         0   PtfmHeave   - Initial or fixed vertical heave translational displacement of platform (meters)
         0   PtfmRoll    - Initial or fixed roll tilt rotational displacement of platform (degrees)
         0   PtfmPitch   - Initial or fixed pitch tilt rotational displacement of platform (degrees)
         0   PtfmYaw     - Initial or fixed yaw rotational displacement of platform (degrees)
--------------------- TURBINE CONFIGURATION ------------------------------
         3   NumBl       - Number of blades (-)
   1.19066   TipRad      - The distance from the rotor apex to the blade tip (meters)
    0.0378   HubRad      - The distance from the rotor apex to the blade root (meters)
         0   PreCone(1)  - Blade 1 cone angle (degrees)
         0   PreCone(2)  - Blade 2 cone angle (degrees)
         0   PreCone(3)  - Blade 3 cone angle (degrees) [unused for 2 blades]
         0   HubCM       - Distance from rotor apex to hub mass [positive downwind] (meters)!!!!
         0   UndSling    - Undersling length [distance from teeter pin to the rotor apex] (meters) [unused for 3 blades]
         0   Delta3      - Delta-3 angle for teetering rotors (degrees) [unused for 3 blades]
         0   AzimB1Up    - Azimuth value to use for I/O when blade 1 points up (degrees)
  -0.09467   OverHang    - Distance from yaw axis to rotor apex [3 blades] or teeter pin [2 blades] (meters)
   0.04734   ShftGagL    - Distance from rotor apex [3 blades] or teeter pin [2 blades] to shaft strain gages [positive for upwind rotors] (meters)!
  -5.00000   ShftTilt    - Rotor shaft tilt angle (degrees)
   0.03580   NacCMxn     - Downwind distance from the tower-top to the nacelle CM (meters)
         0   NacCMyn     - Lateral  distance from the tower-top to the nacelle CM (meters)
   0.03267   NacCMzn     - Vertical distance from the tower-top to the nacelle CM (meters)
  -0.04127   NcIMUxn     - Downwind distance from the tower-top to the nacelle IMU (meters)
         0   NcIMUyn     - Lateral  distance from the tower-top to the nacelle IMU (meters)
   0.02978   NcIMUzn     - Vertical distance from the tower-top to the nacelle IMU (meters)
   0.03667   Twr2Shft    - Vertical distance from the tower-top to the rotor shaft (meters)
   1.54173   TowerHt     - Height of tower above ground level [onshore] or MSL [offshore] (meters)
         0   TowerBsHt   - Height of tower base above ground level [onshore] or MSL [offshore] (meters)
         0   PtfmCMxt    - Downwind distance from the ground level [onshore] or MSL [offshore] to the platform CM (meters)
         0   PtfmCMyt    - Lateral distance from the ground level [onshore] or MSL [offshore] to the platform CM (meters)
        -0   PtfmCMzt    - Vertical distance from the ground level [onshore] or MSL [offshore] to the platform CM (meters)
        -0   PtfmRefzt   - Vertical distance from the ground level [onshore] or MSL [offshore] to the platform reference point (meters)
```

Figure 3.2.4 Elastodyn Input data

The master input file for the Model which is ready for the analysis is configured ,

```
------- FAST v8.16.* INPUT FILE -------------------------------------------------
Wind turbine model of the DTU10MW RWT.
---------------------- SIMULATION CONTROL --------------------------------------
False         Echo            - Echo input data to <RootName>.ech (flag)
"FATAL"       AbortLevel      - Error level when simulation should abort (string) {"WARNING", "SEVERE", "FATAL"}
          4   TMax            - Total run time (s)
       0.01   DT              - Recommended module time step (s)
          2   InterpOrder     - Interpolation order for input/output time history (-) {1=linear, 2=quadratic}
          0   NumCrctn        - Number of correction iterations (-) {0=explicit calculation, i.e., no corrections}
      99999   DT_UJac         - Time between calls to get Jacobians (s)
      1E+06   UJacSclFact     - Scaling factor used in Jacobians (-)
---------------------- FEATURE SWITCHES AND FLAGS ------------------------------
          1   CompElast       - Compute structural dynamics (switch) {1=ElastoDyn; 2=ElastoDyn + BeamDyn for blades}
          1   CompInflow      - Compute inflow wind velocities (switch) {0=still air; 1=InflowWind; 2=external from OpenFOAM}
          1   CompAero        - Compute aerodynamic loads (switch) {0=None; 1=AeroDyn v14; 2=AeroDyn v15}
          0   CompServo       - Compute control and electrical-drive dynamics (switch) {0=None; 1=ServoDyn}
          0   CompHydro       - Compute hydrodynamic loads (switch) {0=None; 1=HydroDyn}
          0   CompSub         - Compute sub-structural dynamics (switch) {0=None; 1=SubDyn}
          0   CompMooring     - Compute mooring system (switch) {0=None; 1=MAP++; 2=FEAMooring; 3=MoorDyn; 4=OrcaFlex}
          0   CompIce         - Compute ice loads (switch) {0=None; 1=IceFloe; 2=IceDyn}
---------------------- INPUT FILES ---------------------------------------------
"WTM/case_ElastoDyn.dat"        EDFile          - Name of file containing ElastoDyn input parameters (quoted string)
"unused"                        BDBldFile(1)    - Name of file containing BeamDyn input parameters for blade 1 (quoted string)
"unused"                        BDBldFile(2)    - Name of file containing BeamDyn input parameters for blade 2 (quoted string)
"unused"                        BDBldFile(3)    - Name of file containing BeamDyn input parameters for blade 3 (quoted string)
"WTM/case_InflowWind.dat"       InflowFile      - Name of file containing inflow wind input parameters (quoted string)
"WTM/case_AeroDyn_WTM.dat"      AeroFile        - Name of file containing aerodynamic input parameters (quoted string)
"unused"                        ServoFile       - Name of file containing control and electrical-drive input parameters (quoted string)
"unused"                        HydroFile       - Name of file containing hydrodynamic input parameters (quoted string)
"unused"                        SubFile         - Name of file containing sub-structural input parameters (quoted string)
"unused"                        MooringFile     - Name of file containing mooring system input parameters (quoted string)
"unused"                        IceFile         - Name of file containing ice input parameters (quoted string)
```

Figure 3.2.5 Final Input file of the model (fst file)

3.3 Compiling of FAST output

Before configuring for output file from FAST, the procedure for running the simulation is explained, The FAST folder location is noted down and Command Prompt(CMD) is started. Directory is to the location of Bin folder in FAST. Then the command to start the FAST simulation and fetching the input file is executed

“ FAST8\bin>FAST_Win32d.exe ..\WTM.fst”

The simulation is done, and the corresponding data is logged to the output file “WTM.out”

'Time'	'Wind1VelX'	'Wind1VelY'	'Wind1VelZ'	'LSSTipPxa'	'LSSTipVxa'	'BlPitch1'	'BlPitch2'	'BlPitch3'	'LSShftMx	'TwrBsFxt'	'YawBrFxp'	'RotPwr'
0	3.8	0	0	0	240	0	0	0	9.50E-10	4.77E-10	4.77E-10	2.39E-08
0.01	3.8	0	0	14.4	240	0	0	0	0.004984	0.04324	0.04324	0.1253

Table 3.3 FAST output file

3.4 Output file parameters

Name	Other Name(s)	Description	Convention	Units
YawBrFxn		Rotating (with nacelle) tower-top / yaw bearing shear force	Directed along the x_n-axis	(kN)
YawBrFyn		Rotating (with nacelle) tower-top / yaw bearing shear force	Directed along the y_n-axis	(kN)
YawBrFzn	YawBrFzp	Tower-top / yaw bearing axial force	Directed along the z_n- and z_p-axes	(kN)
YawBrFxp		Tower-top / yaw bearing fore-aft (nonrotating) shear force	Directed along the x_p-axis	(kN)
YawBrFyp		Tower-top / yaw bearing side-to-side (nonrotating) shear force	Directed along the y_p-axis	(kN)
YawBrMxn		Rotating (with nacelle) tower-top / yaw bearing roll moment	About the x_n-axis	(kN·m)
YawBrMyn		Rotating (with nacelle) tower-top / yaw bearing pitch moment	About the y_n-axis	(kN·m)
YawBrMzn	YawBrMzp YawMom	Tower-top / yaw bearing yaw moment	About the z_n- and z_p-axes	(kN·m)
YawBrMxp		Nonrotating tower-top / yaw bearing roll moment	About the x_p-axis	(kN·m)
YawBrMyp		Nonrotating tower-top / yaw bearing pitch moment	About the y_p-axis	(kN·m)

Table 3.4.1 Tower top and yaw bearing loads parameters.

Name	Other Name(s)	Description	Convention	Units
LSShftFxa	LSShftFxs LSSGagFxa LSSGagFxs RotThrust	LSS thrust force (this is constant along the shaft and is equivalent to the rotor thrust force)	Directed along the x_a- and x_s-axes	(kN)
LSShftFya	LSSGagFya	Rotating LSS shear force (this is constant along the shaft)	Directed along the y_a-axis	(kN)
LSShftFza	LSSGagFza	Rotating LSS shear force (this is constant along the shaft)	Directed along the z_a-axis	(kN)
LSShftFys	LSSGagFys	Nonrotating LSS shear force (this is constant along the shaft)	Directed along the y_s-axis	(kN)
LSShftFzs	LSSGagFzs	Nonrotating LSS shear force (this is constant along the shaft)	Directed along the z_s-axis	(kN)
LSShftMxa	LSShftMxs LSSGagMxa LSSGagMxs RotTorq LSShftTq	LSS torque (this is constant along the shaft and is equivalent to the rotor torque)	About the x_a- and x_s-axes	(kN·m)

Table 3.4.2 Hub and Rotor loads Parameters.

Name	Other Name(s)	Description	Convention	Units
RootFxc1		Blade 1 out-of-plane shear force at the blade root	Directed along the $x_{c,1}$-axis	(kN)
RootFyc1		Blade 1 in-plane shear force at the blade root	Directed along the $y_{c,1}$-axis	(kN)
RootFzc1	RootFzb1	Blade 1 axial force at the blade root	Directed along the $z_{c,1}$- and $z_{b,1}$-axes	(kN)
RootFxb1		Blade 1 flapwise shear force at the blade root	Directed along the $x_{b,1}$-axis	(kN)
RootFyb1		Blade 1 edgewise shear force at the blade root	Directed along the $y_{b,1}$-axis	(kN)
RootMxc1	RootMIP1	Blade 1 in-plane moment (i.e., the moment caused by in-plane forces) at the blade root	About the $x_{c,1}$-axis	(kN·m)
RootMyc1	RootMOoP1	Blade 1 out-of-plane moment (i.e., the moment caused by out-of-plane forces) at the blade root	About the $y_{c,1}$-axis	(kN·m)
RootMzc1	RootMzb1	Blade 1 pitching moment at the blade root	About the $z_{c,1}$- and $z_{b,1}$-axes	(kN·m)
RootMxb1	RootMEdg1	Blade 1 edgewise moment (i.e., the moment caused by edgewise forces) at the blade root	About the $x_{b,1}$-axis	(kN·m)
RootMyb1	RootMFlp1	Blade 1 flapwise moment (i.e., the moment caused by flapwise forces) at the blade root	About the $y_{b,1}$-axis	(kN·m)

Table 3.4.3 Blade 1 root loads parameters

Name	Other Name(s)	Description	Convention	Units
LSSTipPxa	LSSTipPxs LSSTipP Azimuth	Rotor azimuth angle (position)	About the x_a- and x_s-axes	(deg)
LSSTipVxa	LSSTipVxs LSSTipV RotSpeed	Rotor azimuth angular speed	About the x_a- and x_s-axes	(rpm)
LSSTipAxa	LSSTipAxs LSSTipA RotAccel	Rotor azimuth angular acceleration	About the x_a- and x_s-axes	(deg/sec^2)

Table 3.4.4 Shaft Motion parameters

3.5 Configuring output file to MATLAB

The output file is fetched, and the corresponding output parameters are used to plot the average values and time series plots which are used for the further analysis.

4 Interpretation of output data

At first a Static thrust plot describing wind speed vs the blade Force of DTU RWT is considered ,as shown in figure 4.1.3 rated wind speeds and Rotor speed were chosen with run time of 4seconds with 400 samples, the average thrust force of each point is obtained by altering the pitch angle of the blade until it matches with force of the DTU RWT. So the matching points can be used for further examination in measuring the blade forces with added conditions.

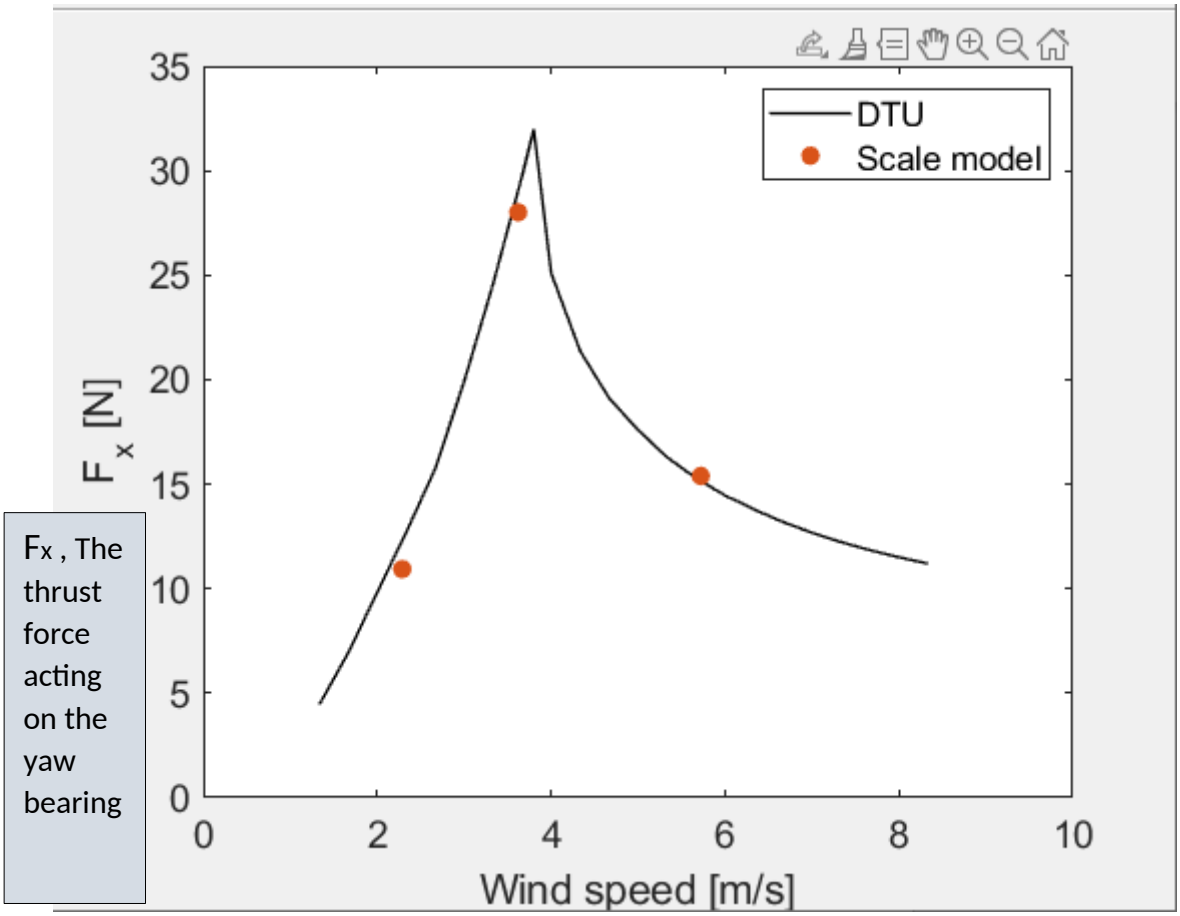

F_x , The thrust force acting on the yaw bearing

Figure 4.1 Static thrust curve

The DTU RWT's specifications of the 3 conditions is given in the table 4.1(a) and the corresponding WTM model's matching curve specifications is noted in the table 4.1. (b)

Wind speed	Rot. Speed	Blade Pitch	Fx (N)
2.33 m/s	150 rpm	-4 deg	10.9416 N
3.67 m/s	221 rpm	-4 deg	28.0109 N
5.33 m/s	240 rpm	10.75 deg	15.3980

a) Specific point DTU RWT Parameters

Wind speed	Rot. Speed	Blade Pitch (degree)	Fx(N)
2.33 m/s	150rpm	**2.3**	10.96974
3.67 m.s	221rpm	**1.3**	28.0387
5.33 m/s	240 rpm	**14**	15.17036

b) WTM model's parameters

Table 4.1 Final matching pitch results.

Then further the test is expanded to recreate the exact curve with more points and resultant graph is shown in the figure 4.2.Also the resultant average bending moments of these points are plotted along with wind speed as shown in the figure 4.3.

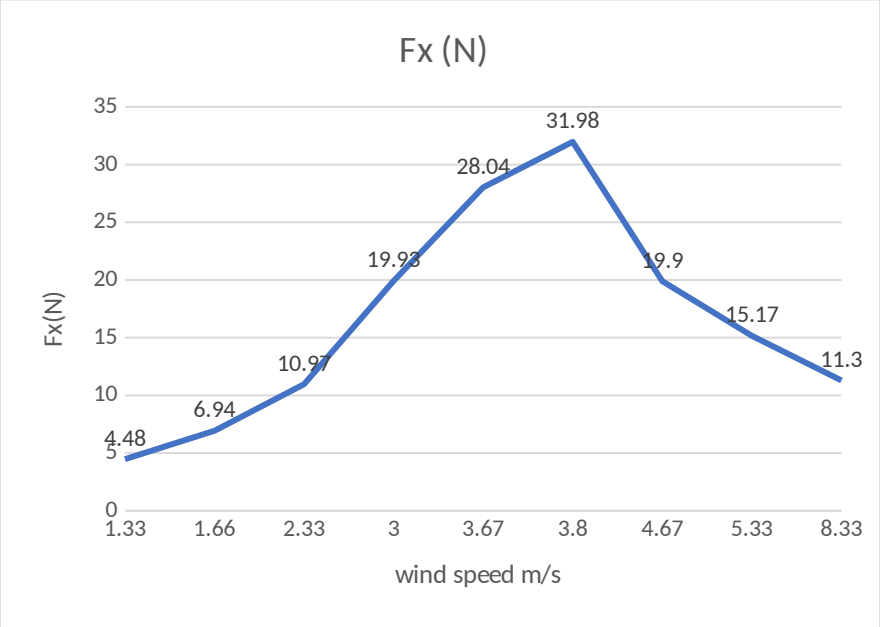

Figure 4.2 Recreation of the static curve of the model.

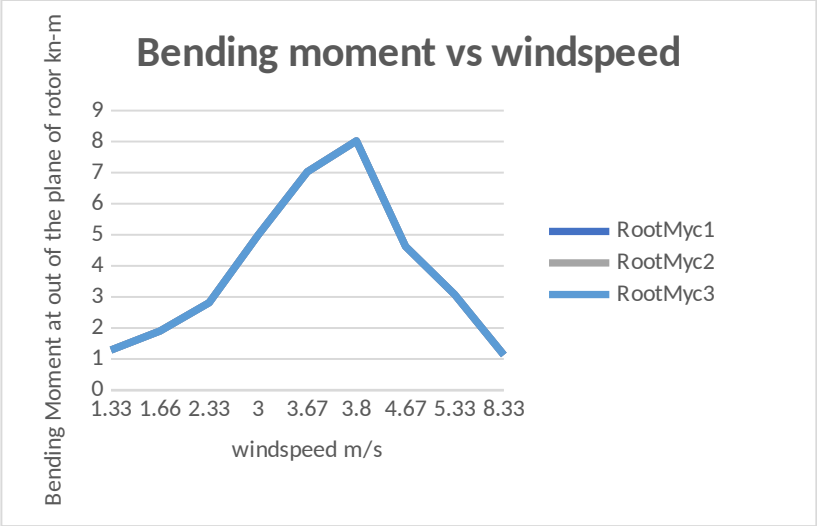

Figure 4.3 Out of the plane bending moment(avg) vs wind speed plot.

Then the out of the plane bending moment of the 3 conditions as mentioned in the table 4.2 is plotted in time series as shown in the figure 4.4.

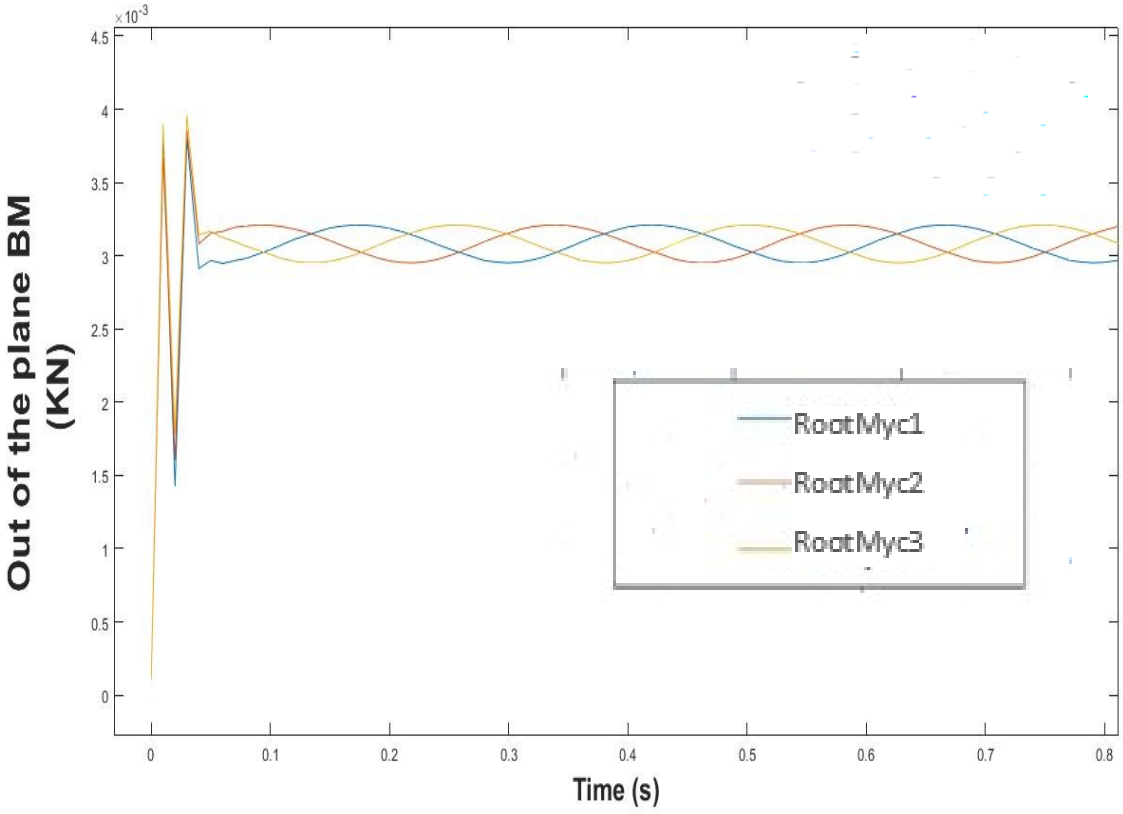

(a) Condition 1

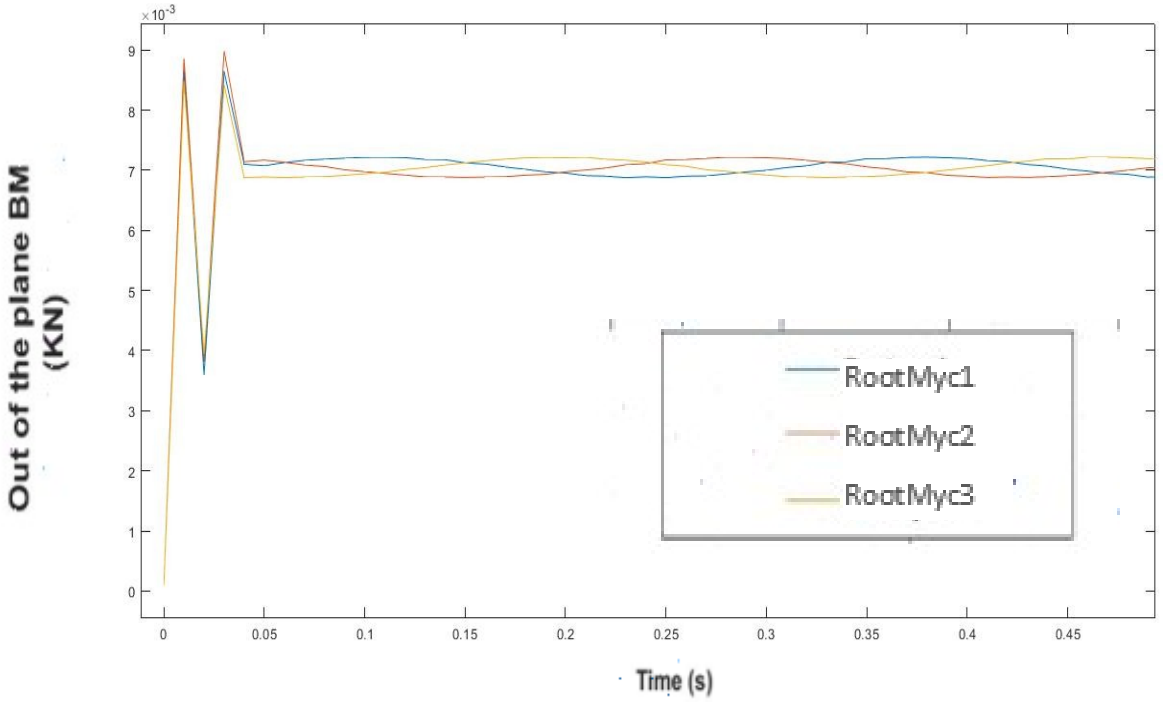

(b) Condition 2

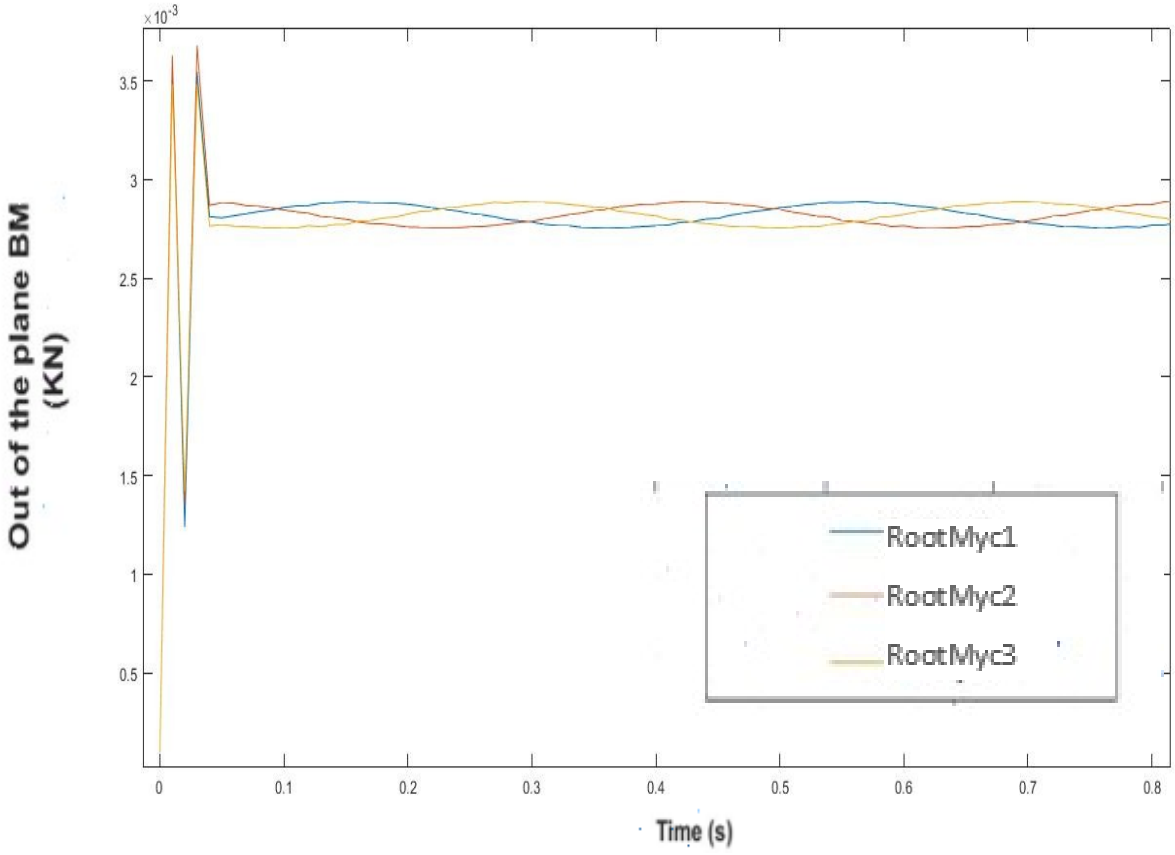

(c) Condition 3

Figure 4.4 Bending moment vs Time plot

The figure 4.4 interprets the time series plot of the out of the plane bending moment at root of the three blades at each condition we chose for the recreation for the thrust matching curve. After 0.06 seconds the bending moments follows a periodic pattern, but in the lower wind case(2.33 m/s), the blade 1 moment seems to less at the periodic starting time, compared to other rated wind speeds.

4.1 MBC(Coleman) Transformation for wind turbine load reduction

The rotors of wind-turbine generators (WTGs) are known to be subjected to considerable unbalanced and variable loads due to gravity force, wind shear, yaw error, tower shadow, and atmospheric turbulence in the wind energy industry. These forces provide unsteady mechanical stresses on the blade roots, which are then transferred to the hub and other non-rotating turbine structures (e.g. main bearing, yaw bearing, nacelle, and tower), resulting in unsteady tilt and yaw loads on the main structure of the turbine. If not properly managed, such loads can cause fatigue and shorten turbine lifetime.

The majority of control strategies assume a steady and uniform wind over the rotor plane. A coordinate transformation technique known as the Coleman transformation is used in the majority of extant IPC research. This evolution may be traced back to the realm of helicopter rotor control,[32] and similar techniques such as Individual blade-pitch control[33] Q. Lu, R. Bowyer and B. Ll. Jones the d-q transformation are also employed in the field of electrical machines and power electronics.[33] Previous adoption of the Coleman transformation for dealing with IPC problems was reported by Bossanyi6 and Van Engelen and Van der Hooft.[35] The basic idea is to project rotating blade loads onto a set of non-rotating locations, resulting in orthogonal tilt and yaw stresses. The blade loads can therefore be lowered by constructing separate controllers to reduce the tilt and yaw loads, albeit this requires some caution due to the non-trivial mapping of load frequencies between rotating and fixed turbine structures.

The unstable stresses faced by WTGs are concentrated at certain harmonics, as discovered by Barlas and Van Kuik1. The blade loads contain harmonics at 1p (once per revolution), 2p, 3p, and other frequencies, whereas the loads on the non-rotating turbine structure only contain harmonics at 3p, 6p, and other frequencies for three-bladed turbines. [34] At frequency multiples of 3p, the remaining harmonics on the non-rotating turbine structure are transferred to their adjacent harmonics. [8] Harmonics on the rotating coordinate, for example, are translated to 0p (static content) on the non-rotating coordinate, whereas 2p and 4p harmonics are transferred to the 3p harmonic. Because of the links between the loads on the blades and the non-rotating turbine structure, it is possible to build a single controller that can reduce these loads concurrently and over a wide frequency range. The Coleman

transformation is appealing from the standpoint of controls design because it converts a time-periodic and thus time-varying system into one that is time invariant.

Furthermore, if the system dynamics are linear or can be approximated as such, the resulting WTG model is linear and time invariant (LTI), allowing a large body of mature and sophisticated control systems theory to be used to the design of IPCs right away. [37] The Coleman transformation also has the critical virtue of allowing the IPC to be separated from an existing CPC in terms of control system design. [37],[38] The goal here was to reduce the static content of the tilt and yaw loads while also lowering the 1p blade loads. This method, however, ignored all other higher-frequency disturbance loads, such as the 3p content of tilt and yaw loads, which have been discovered to be the primary cause of fatigue-induced damage on non-rotating turbine structures. [39],[40] to deal with the control of these high frequency loads.

These changes were made using a modified Coleman transformation' concept, in which the process of demodulation and remodulation for higher blade load frequencies (2p, 3p, etc.) was defined, and these higher frequencies were modulated to 0p and then attenuated using the traditional 1p load reduction approach. To attenuate the 0p content in the modulated loads, two independent proportional-integral (PI) controllers were commonly used to manage these blade load frequencies (i.e., 1p, 2p, 3p, etc.).

Using such single-input–single-output (SISO) controllers, however, implicitly assumes that the tilt and yaw dynamics are decoupled after application of the Coleman transform, which was shown not to be the case by Selvam et al.[37] and Geyler and Caselitz[38], who found dynamic tilt–yaw coupling with the degree of coupling heavily influenced by the rotor speed.

4.2 Model for the transformation analysis

Figure 4.2.1 shows a Coleman transformation-based IPC's conceptual control systems architecture. IPC and CPC are usually implemented separately, with the former's design based on one of the control techniques such as PID, LQG, and so on. Standard turbine models typically contain the dynamics of the stationary and rotating turbine components, and are thus time variable in character due to the changing angular orientation of the rotating blades in model-based control design techniques.

Additional inputs to the turbine, such as wind loading and generator torque are accounted. The system within the shaded region represents the Coleman transformed turbine, whose dynamics are linear and time invariant once the turbine model is linearized around a fixed operating point.

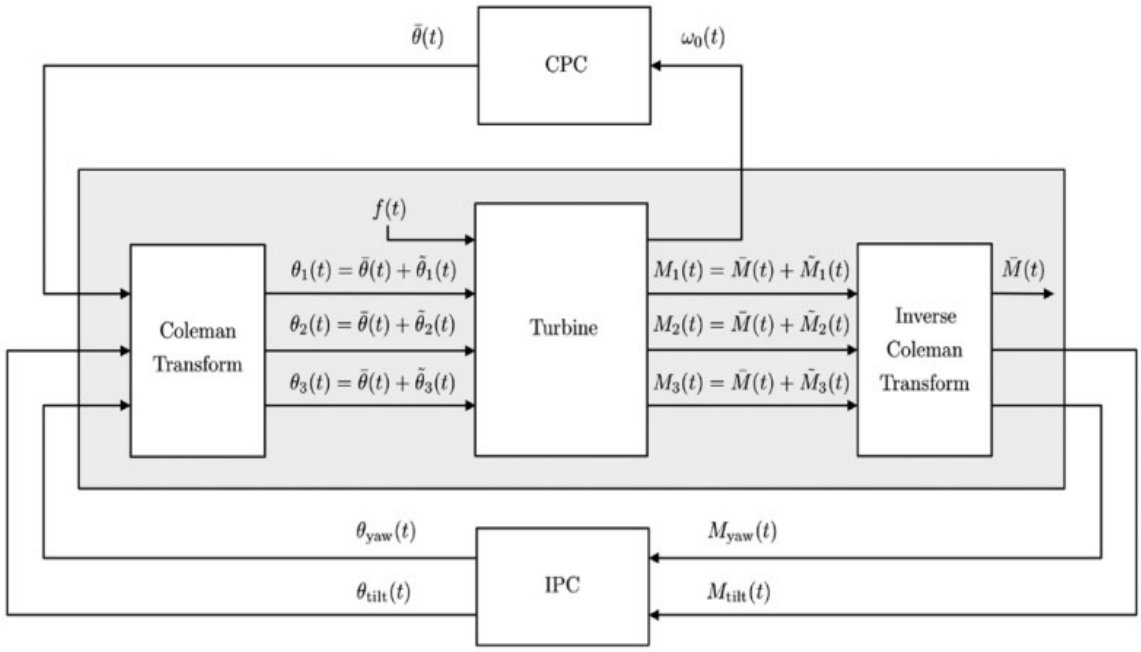

Figure 4.2.1 Systems architecture of a Coleman transformation-based IPC

[37] A transformed system defined in a fixed coordinate frame is obtained by applying the Coleman transformation to the inputs and the inverse Coleman transformation to the outputs of the rotational system, linking blade-pitch angles to blade root bending moments. Because such a system is time invariant, it may be designed using ordinary feedback control techniques. The collective pitch controller computes the averaged blade-pitch angle requirement theta(t) for managing the rotor speed omega(t) as shown in Figure 4.2.1. The overall pitch angle needs on each blade are calculated using the Coleman transform, coupled with the tilt and yaw referenced pitch angles YawBrMyp and YawBrMzp. and the demand theta1,2,3.(t).

$$\begin{pmatrix} \text{Theta1} \\ \text{Theta2} \\ \text{Theta3} \end{pmatrix} = \begin{pmatrix} 1 & \cos(\text{LSSTipPxa}) & \sin(\text{LSSTipPxa}) \\ 1 & \cos(\text{LSSTipPxa}+2*\text{pi}/3) & \sin(\text{LSSTipPx})+2*\text{pi}/3) \\ 1 & \cos(\text{LSSTipPxa}+4*\text{pi}/3) & \sin(\text{LSSTipPxa}+4*\text{pi}/3) \end{pmatrix} \begin{pmatrix} \text{Theta}\sim \\ \text{YawBrMyp} \\ \text{YawBrMzp} \end{pmatrix}$$

Equation 1

The rotor azimuth angle is LSSTipPxa(t). The total blade root flap-wise bending moments, M1,2,3.(t), which are related to the tilt and yaw moments, Mtilt(t) and Myaw(t), are essential turbine outputs (t).

4.2.1 Frequency domain representation of the transformation:

With respect to equation (1), linearization removes explicit dependence of the turbine model upon the averaged quantities Because of theta(t) and M(t), just the tilt and yaw signals in the fixed reference frame require attention. As a result, the Coleman relationships relevant to the IPC problem are a subset of equation (1), and they are defined as follows:

$$\begin{bmatrix} \text{Theta} \end{bmatrix} = \begin{bmatrix} \cos(\text{LSSTipPxa}) & \sin(\text{LSSTipPxa}) \\ \cos(\text{LSSTipPxa} + 2*\pi/3) & \sin(\text{LSSTipPxa}+2*\pi/3) \\ \cos(\text{LSSTipPxa})+4*\pi/3) & \sin(\text{LSSTipPxa}+4*\pi/3) \end{bmatrix} \begin{bmatrix} \text{YawBrMyp} \\ \text{YawBrMzp} \end{bmatrix}$$

Equation 2

The equation 2 represents the transformation of measured data from the fixed parts(tower top) to the rotating parts (Blades)

$$\begin{bmatrix} \text{Mtilt} \\ \text{Myaw} \end{bmatrix} = 2/3 \begin{bmatrix} \cos(\text{LSSTipPxa}) & \cos(\text{LSSTipPxa}+2*\pi/3) & \cos(\text{LSSTipPxa}+4*\pi/3) \\ \sin(\text{LSSTipPxa}) & \sin(\text{LSSTipPxa}+2*\pi/3) & \sin(\text{LSSTipPxa}+4*\pi/3) \end{bmatrix} * \begin{bmatrix} \text{RootMyc1} \\ \text{RootMyc2} \\ \text{RootMyc3} \end{bmatrix}$$

Equation 3

The equation 3 represents the inverse transformation of the measured data from the rotary parts to the fixed parts.

Now the values at the tower top load and Blade root from the simulation is interpreted through the MATLAB. The task it to investigate whether the MBC transformed blade root bending moment is similar to the measured bending moment at the tower top loads or to Examine the MBC transformed Tower top moment with the measured blade loads.

The examination is done with 2 wind flow condition , steady and turbulent flow. The respected result of the task is plotted and discussed below:

Condition 1:

The wind flow utilized here is Stead flow, with speed of 3.67 m/s. The pitch angle is 1.3 degrees with rotor speed of 221 rpm. The shaft tilt angle is altered with 0 and -5 degrees. Combinations of gravity and tilt angle were used for analysis and plotted.

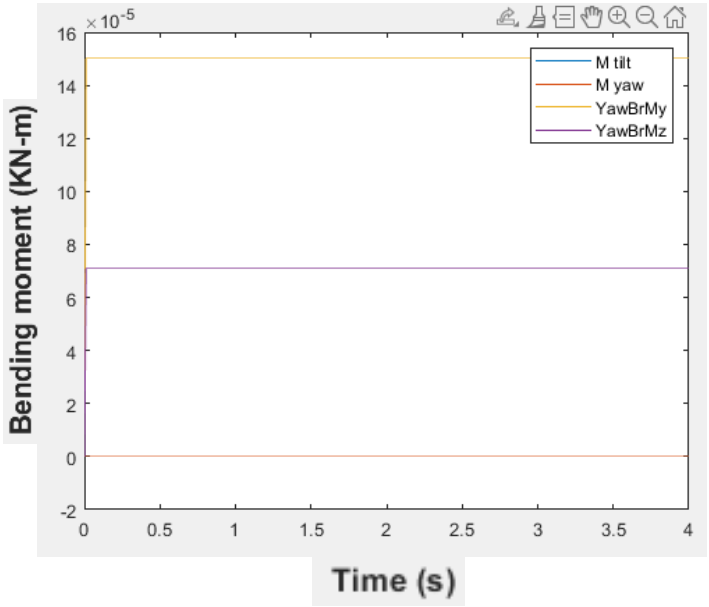

a) (-5) tilt angle, zero_grav

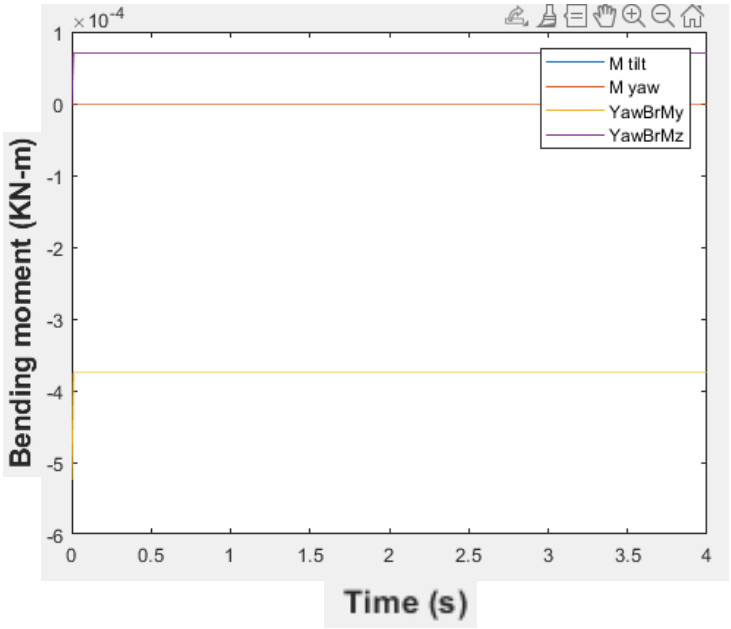

b) (-5)tilt angle, gravity

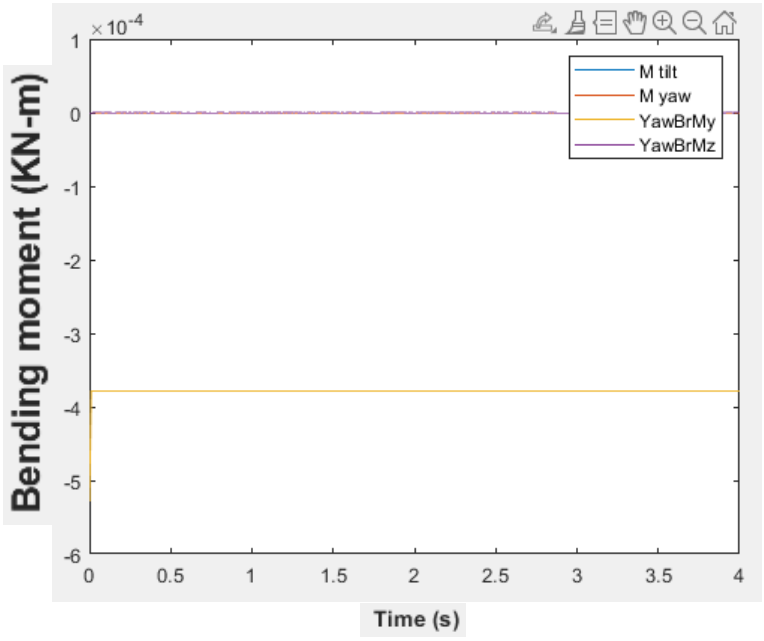

c) ZERO_TILT, GRAV

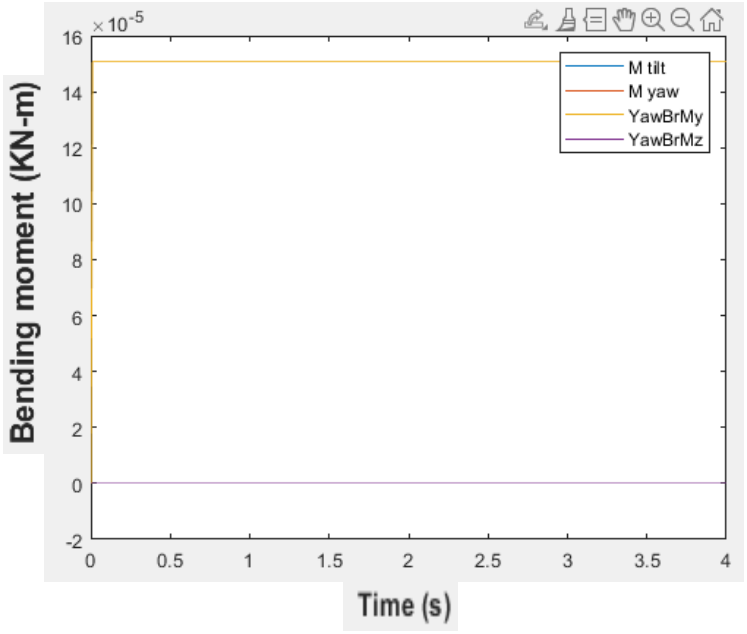

d) zero_tilt, zero_grav

Figure 4.2.2 Mtilt,Myaw,Yawbrmyp,yawbrmzp vs time

The figure 4.2.2 denotes the graph of bending moments at tower top and the Multi blade coordinates transformed bending moment from the root of the blades vs time.

Where with '"a) zero gravity and -5 degree tilt angle"- the transformed bending moments are zero and the tower top moments are non-zero.

In "(b) gravity and -5 tilt angle" in the experiment -its same considering previous condition ,but there is a significant reduction in the tower top loads.

In "(c) Zero tilt angle and presence of gravity", the Y-moments at the tower top is alone non-zero and rest of the moments are zero.

In"(d) zero tilt angle and zero gravity "condition, its same as the (c) condition but the Y-moment of tower top is high compared to the previous one.

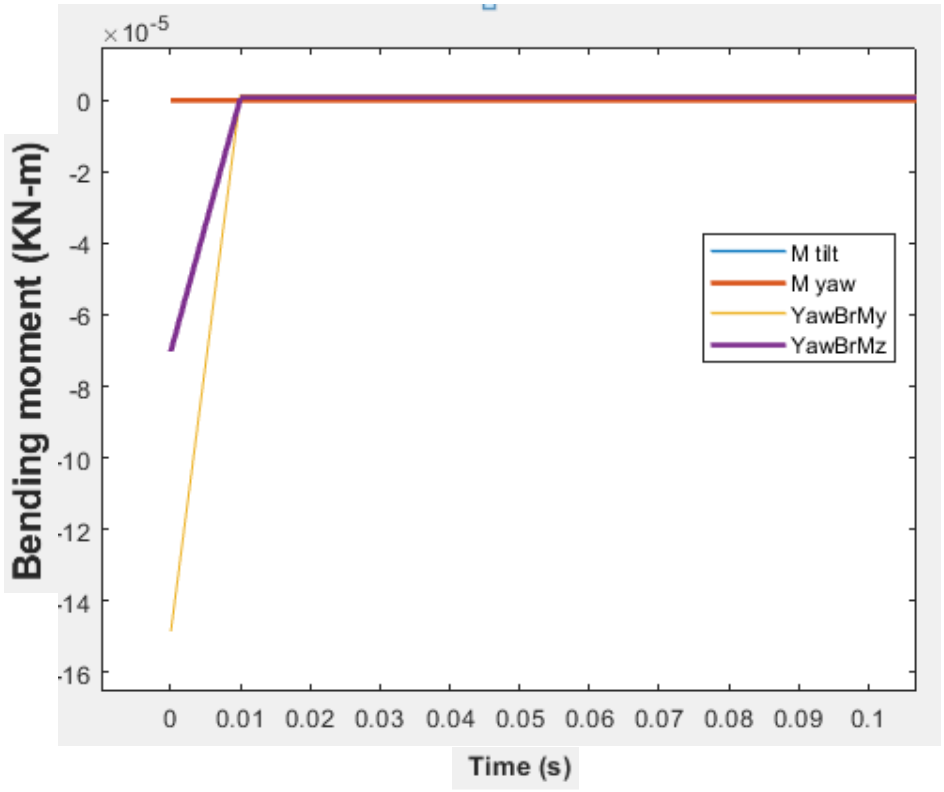

a) tilt angle(-5) and zero_grav

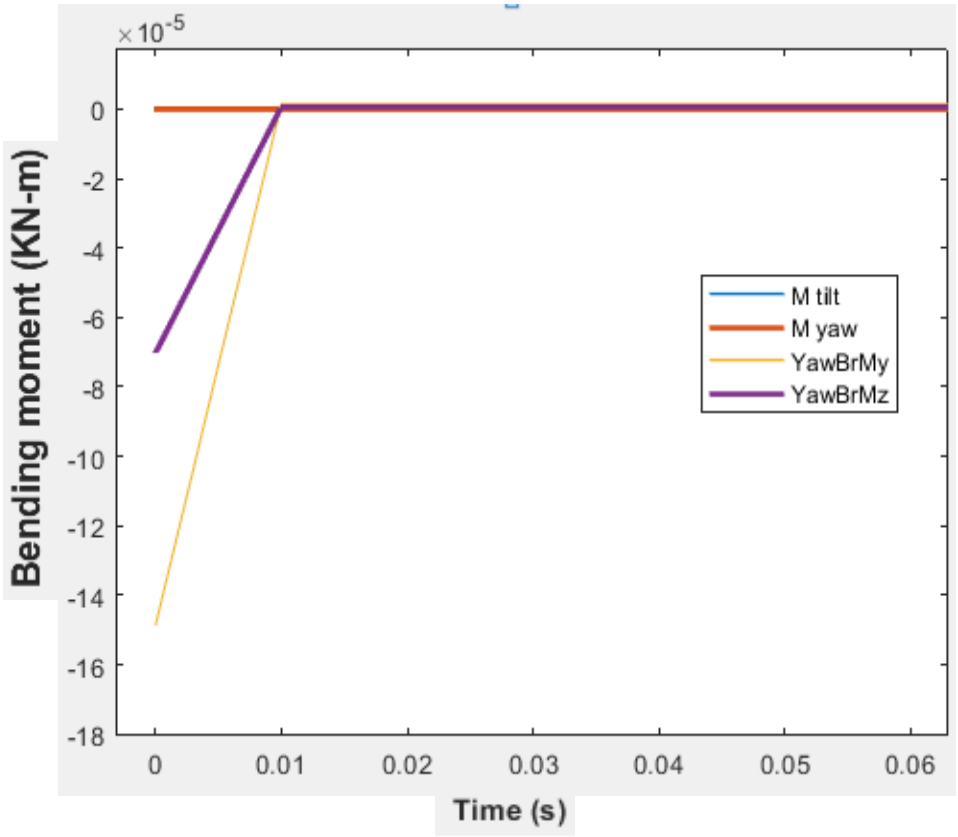

b) (-5)tilt angle and gravity

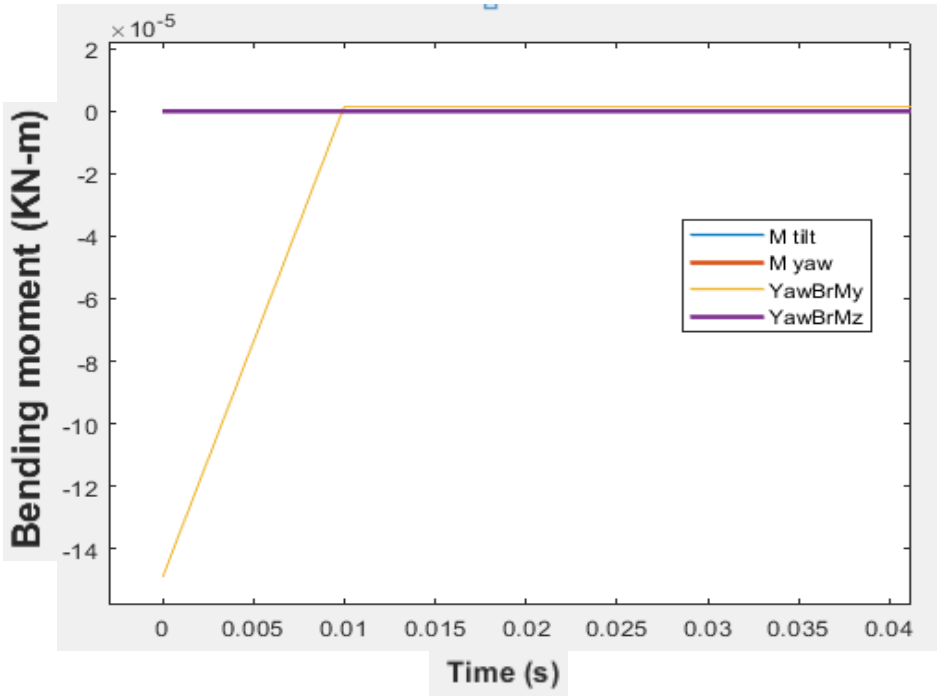

c) ZEROTILT,GRAV

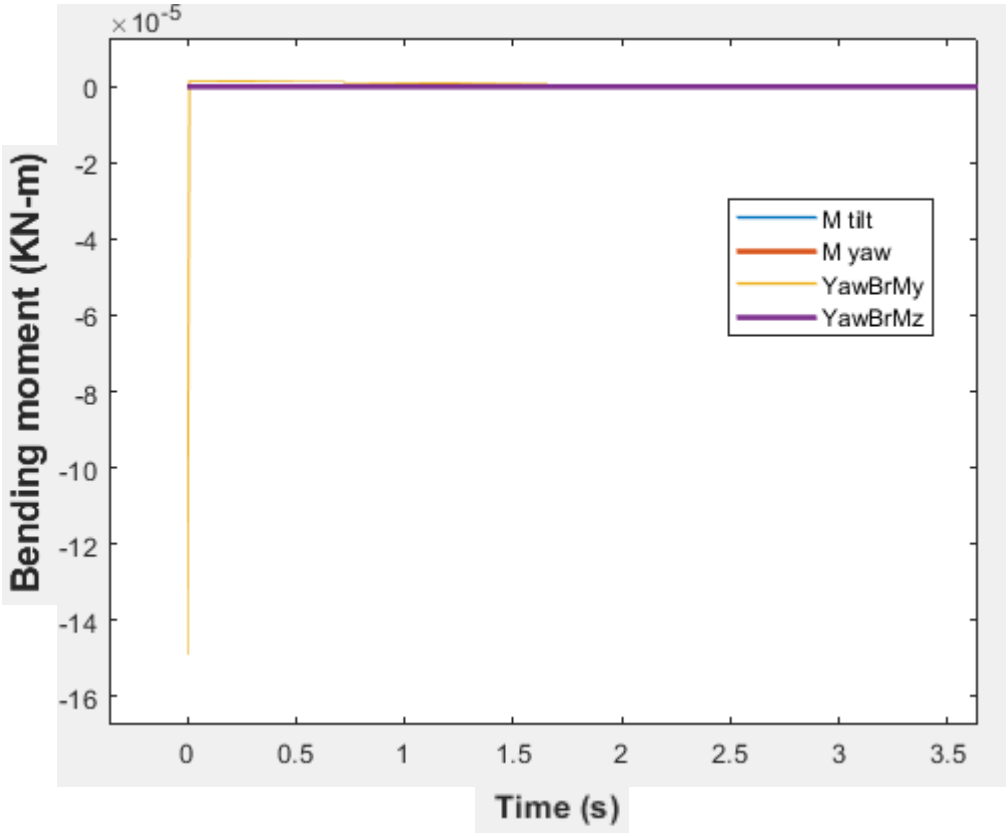

d) zero_tilt, zero_grav

Figure 4.2.3 Detrended Bending moment VS time

The figure 4.2.3 interprets the time series plot of the detrend bending moment of Tower top loads and MBC transformed loads. The difference of YawBrMy moment is due to the overhanging of the rotor. Among these graphs, condition d) shows aimed pattern of the bending moments. Hence zero gravity and zero tilt angle can be sued for further analysis.

Condition 2:

The wind flow utilized here is turbulent flow, with speed of 3.67 m/s. The pitch angle is 1.3 degrees with rotor speed of 221 rpm. The shaft tilt angle is altered with 0 and -5 degrees and combined with and without gravity. The power spectrum analysis is carried out in this part for the turbulent flow conditions.

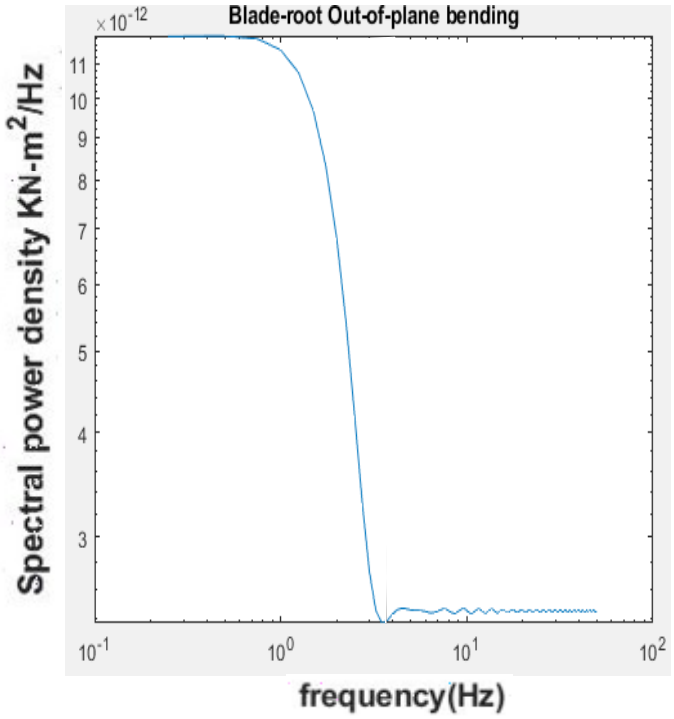

(a) (-5)tilt angle and zero_grav

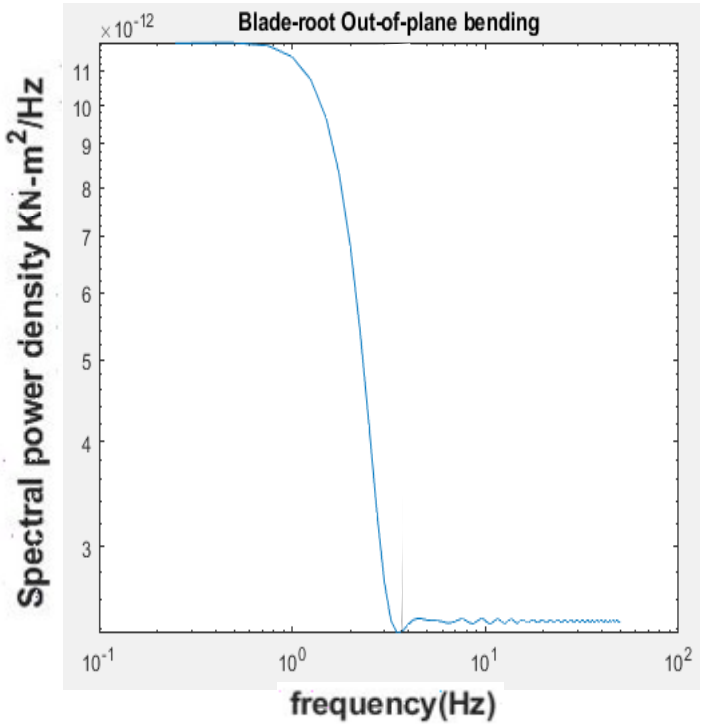

(b) (-5)tilt angle with gravity

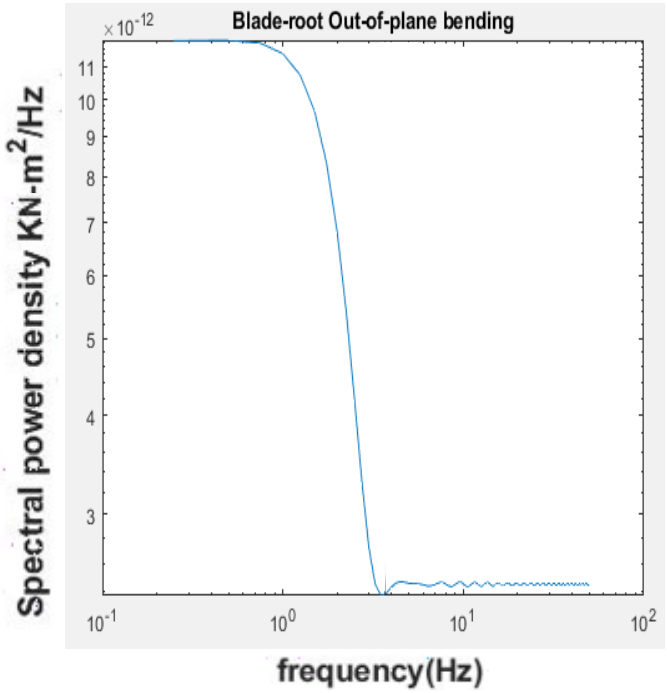

(c) Zero tilt angle, gravity

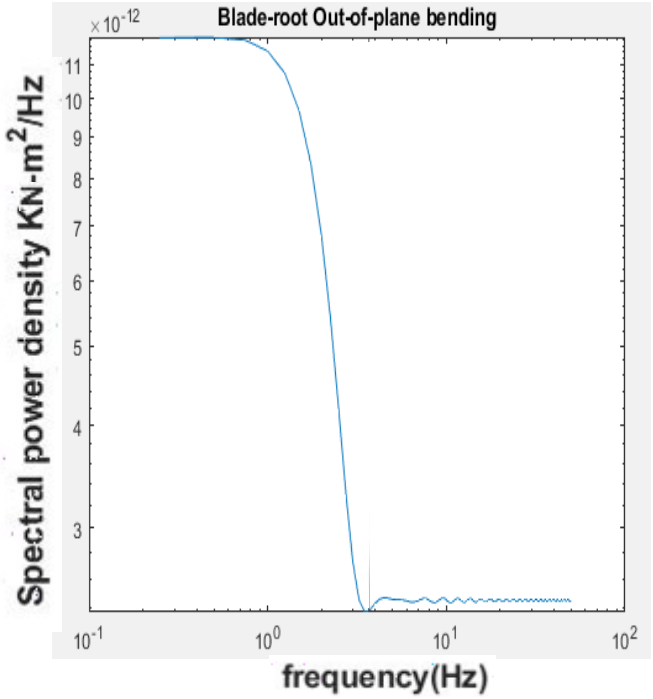

(d) Zero tilt angle ,zero gravity

Figure 4.2.4 Power spectrum of Bending moment of blade 1

Figure 4.2.4 represents the spectral density plot of “out of the plane bending moment of blade_1”. The bending moment variation at the blade is similar in all the shaft tilt and gravity conditions.

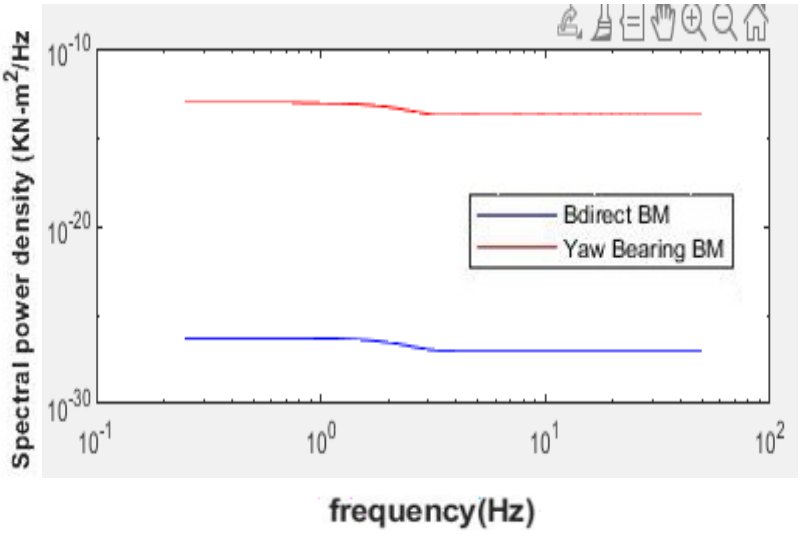

a) (-5)tilt angle and zero gravity

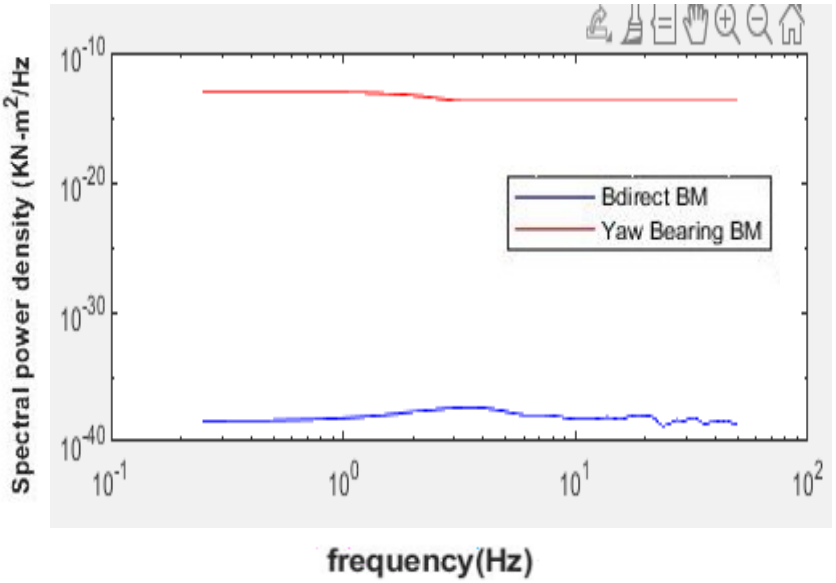

b) (-5) tilt angle with gravity

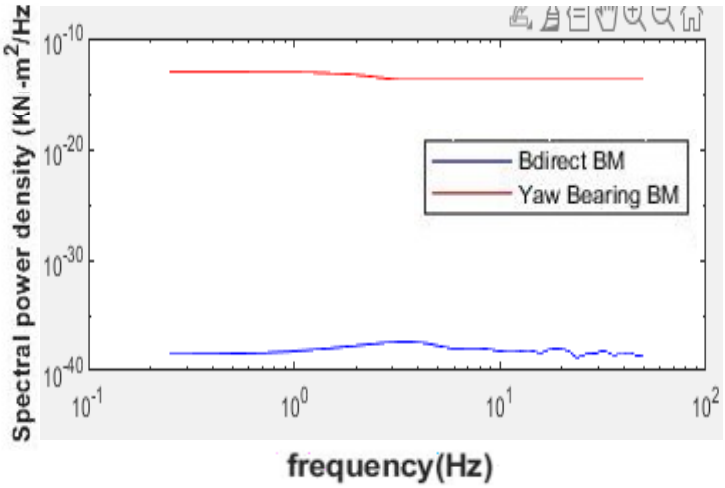

c) Zero tilt angle with Gravity

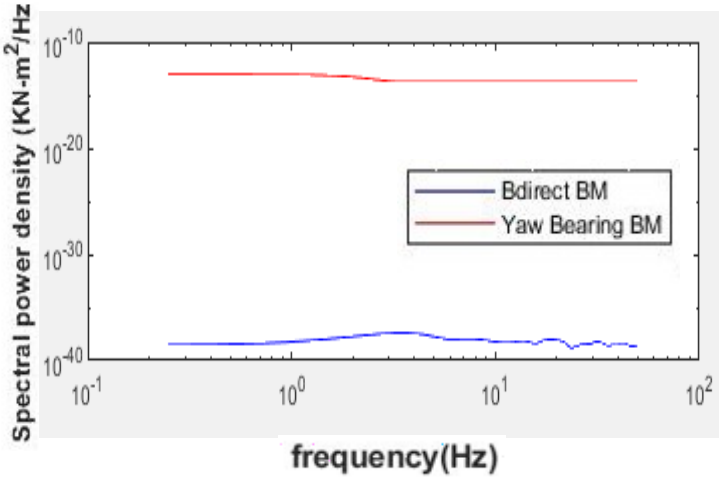

d) Zero tilt angle and zero gravity

Figure 4.2.5 Power spectrum comparison of Tower top Y-moment and M-tilt moment

Figure 4.2.5 represents the power spectrum comparison of Yaw Bearing(Y) Bending moment with the MBC transformed (M tilt) bending moment at the root of the blades. In the zero gravity and tilt angle of -5 degrees , the transformed bending moment(M tilt) has less variation and low power distribution in all frequencies compared with other graphs . The power distribution curve of Mtilt and Yaw bearing bending moment are similar in this condition(a) alone.

5 d-q Axis Transformation

This technique tries to eliminate asymmetric loads caused by wind speed fluctuations across the rotor disc, which are becoming increasingly significant as turbine rotors become larger in comparison to typical turbulent eddies in the wind. Other measurements, such as accelerometers in each blade tip or lateral and vertical accelerometers in the nacelle, could be employed instead. [42]

Wind shear, tower shadow, yaw misalignment, and turbulence cause changes in wind speed and direction as the turbine blade sweeps around the 'rotor disc.' The impact of turbulent wind speed fluctuations across the rotor disc grows as rotor sizes grow in relation to the typical sizes of turbulent eddies.

These changes cause the blade loads to have a substantial once-per-revolution, or 1P, component, as well as harmonics of this frequency, such as 2P, 3P, 4P, and so on. With a three-bladed rotor, these load components will be 120° out of phase between the three blades, resulting in harmonics at 3P, 6P, and so on, which will be felt by the hub and the rest of the structure, but 1P and the other harmonics will tend to cancel out. [42]

Decoupling the collective from the differential or 1P pitch action yielded the best results. A normal classical PI-based controller is used to calculate the collective pitch action, which is the same for all three blades, and a zero-mean 1P differential pitch action is superimposed on this to lower the 1P loads. A multivariable controller having at least two inputs (measurements) and two outputs is required for differential pitch action. The three pitch demands are made up of a collective pitch requirement and two distinct differential needs, despite the fact that there are three blades.

Three blade root load signals are translated into a mean value and variations about two orthogonal axes (the 'direct' and' quadrature' axes), which could represent the vertical and lateral directions, for example, using the d–q axis representation adopted from three-phase electrical machine theory3. The differential pitch 'outputs' in the d- and q-axes are then calculated, and the differential demands for the three blades are obtained by a reverse transformation. [42]

It has been demonstrated that the d- and q-axes can be treated as almost independent. This means that traditional design techniques may be used to create a single-input, single-output controller that can be used on the d-axis and q-axis separately. A simple filter in series with a traditional PI controller gives excellent control action. There is some interaction between the two axes in practice, but this may be accounted for by adding a simple azimuthal phase shift to the d–q axis transformation, i.e. adding a constant offset to the rotor azimuth angle used in the transformation.

The transformation of the d–q axis is as follows:

(1) Transformations of direct and quadrature axes from three rotating blades:

$$\begin{pmatrix} \beta_d \\ \beta_q \end{pmatrix} = \left(\frac{2}{3}\right) \begin{pmatrix} \cos(\theta) & \cos(\theta + 2\pi/3) & \cos(\theta + 4\pi/3) \\ \sin(\theta) & \sin(\theta + 2\pi/3) & \sin(\theta + 4\pi/3) \end{pmatrix} \begin{pmatrix} \beta_1 \\ \beta_2 \\ \beta_3 \end{pmatrix}$$

Equation 4

where beta1 –beta3 are quantities referred to blades 1–3 respectively, betad and betaq are referred to the direct and quadrature axes respectively and theta is the angle between blade 1 and the direct axis direction.

(2) Transformations from direct and quadrature axes back to three rotating blades

$$\begin{pmatrix} \beta_1 \\ \beta_2 \\ \beta_3 \end{pmatrix} = \begin{pmatrix} \cos(\theta) & \sin(\theta) \\ \cos(\theta + 2\pi/3) & \sin(\theta + 2\pi/3) \\ \cos(\theta + 4\pi/3) & \sin(\theta + 4\pi/3) \end{pmatrix} \begin{pmatrix} \beta_d \\ \beta_q \end{pmatrix}$$

Equation 5

The vertical and lateral directions for the direct and quadrature axes are useful because they produce an axis system that is fixed in space. Wind speed fluctuations are rare in this co-ordinate system, and rotational sampling has no effect. The rotor azimuth angle is then theta. If blade loads are detected, they are converted into d–q axes using the forward transformation (1). If spinning hub or shaft loads are applied, all that is necessary is a simple rotational transformation across the azimuth angle. The d–q axis co-ordinate system can already contain loads sensed on a fixed part of the turbine, such as the main bearing housing or the yaw bearing. Further the transformation is carried out in our model analysis

Input parameters:

Here we are considering a turbulent wind flow and wind speed of 3.67 m/s, pitch angle is 1.3 degrees , rotor speed of 221 rpm and shaft tilt angle and gravity is kept 0.

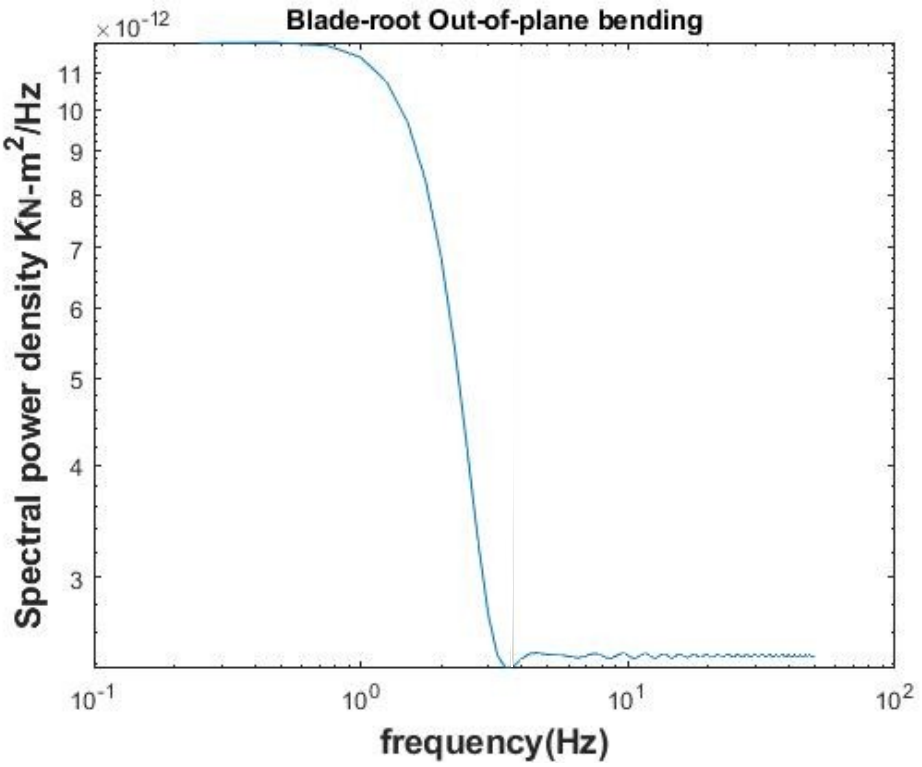

Figure 5.1 Power spectrum of Blade 1 out of the plane bending moment

The graph in the figure 5.1 represents that power spectrum of the Blade 1 out of the plane bending moment. Where at lower frequency the variations are stronger with high bending moment ,then it gradually falls down with increasing frequency range.

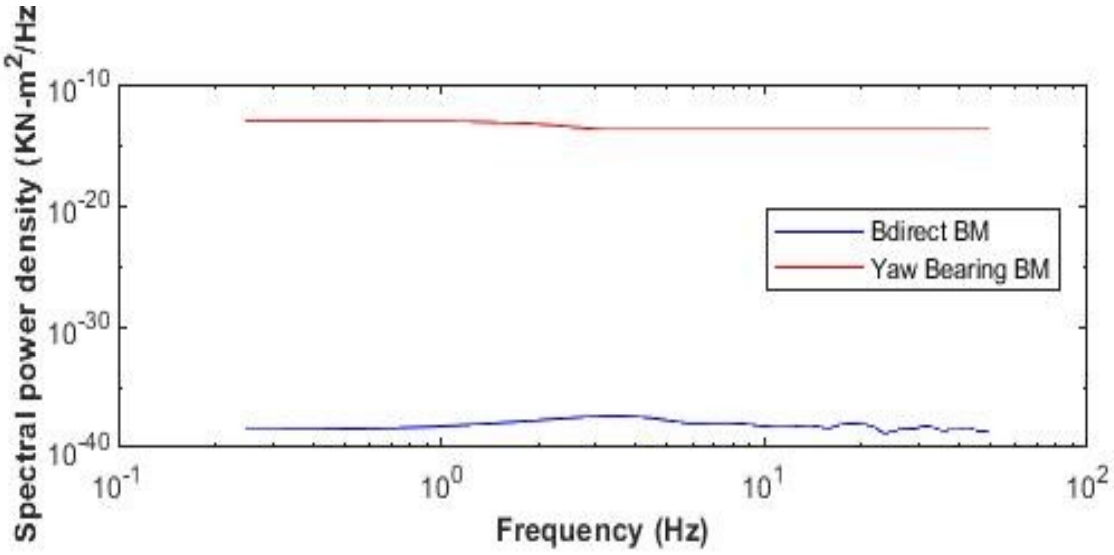

Figure 5.2 Power spectrum of Tower top load vs Direct axis transformed bending moment

The graph, Figure 5.2 represents the power spectrum comparison of Yaw Bearing(Y) Bending moment with the transformed Direct axis bending moment at the root of the Blades. It shows that the direct axis bending moment which is transformed from the rotary parts has less moment power distribution compared to bending moment at tower top i.e, yaw bearing.

6 Conclusion

- From the Plots, we can conclude that In MBC transformation the bending moment power spectra of tower top load and MBC transformed bending moment, shows that the condition of tilt angle -5 degree and zero gravity has similar distribution of moments, but time series show it possess higher bending moment at the tower top compared to other categories. Thus, the similarity is considered, also with zero gravity and zero tilt condition figure 4.2.3 (d), we found similar curve in time graph .
- But our goal is to match the tower top moment values with the transformed values of root of the blade. The same condition(d) is applied to d&q transformation for further analysis.
- In d&q transformation, we found out that it also shows near similarity results like MBC transformation. The reconstruction of simulated root blade loads varies with the transformed tower top loads slightly .
- The future work is divided in two ways
  - i) To re-model the blade design and dimensions until it matches the loads values,
  - ii) Or to apply new algorithm to reduce the offset and variations of the values until it matches with target values.

Appendix

7.1 MATLAB codes

7.1.1 Code for MBC transformation

```
clear
close all
clc

% FAST output
FileName = 'WTM_turb_zerotilt.out';
[Channels, ChanName, ChanUnit,DescStr] = ReadFASTtext(FileName);

Time      = Channels(:,strmatch('Time',ChanName));
RootMyc1  = Channels(:,strmatch('RootMyc1',ChanName));
RootMyc2  = Channels(:,strmatch('RootMyc2',ChanName));
RootMyc3  = Channels(:,strmatch('RootMyc3',ChanName));
YawBrMyp  = Channels(:,strmatch('YawBrMyp',ChanName));
YawBrMzp  = Channels(:,strmatch('YawBrMzp',ChanName));
LSSTipPxa = Channels(:,strmatch('LSSTipPxa',ChanName))*pi/180;
LSSTipVxa = Channels(:,strmatch('LSSTipVxa',ChanName));

%
% YawBrMyp0 = -5.255E-04;
% YawBrMyp  = YawBrMyp - YawBrMyp0;

% MBC transform
for ii = 1:size(Channels,1)

    % Rotating to fixed
    M = [RootMyc1(ii); RootMyc2(ii); RootMyc3(ii)];

    T = 2/3*[cos(LSSTipPxa(ii)),cos(LSSTipPxa(ii)+2*pi/3),cos(LSSTipPxa(ii)+4*pi/3);
             sin(LSSTipPxa(ii)),sin(LSSTipPxa(ii)+2*pi/3),sin(LSSTipPxa(ii)+4*pi/3)];

    Mf(ii,:) = T*M;


    % Fixed to rotating
    thetaf = [YawBrMyp(ii); YawBrMzp(ii)];

    Tpi = [cos(LSSTipPxa(ii)),       sin(LSSTipPxa(ii));
           cos(LSSTipPxa(ii)+2*pi/3),sin(LSSTipPxa(ii)+2*pi/3);
           cos(LSSTipPxa(ii)+4*pi/3),sin(LSSTipPxa(ii)+4*pi/3)];

    theta(:,ii) = Tpi*thetaf;

end

figure(1)
```

```
plot(Time,RootMyc1,Time,RootMyc2,Time,RootMyc3)
legend('OoP 1','OoP 2','OoP 3')
% xlim([98 100])

figure(2)
plot(Time,Mf(:,1),Time,Mf(:,2),Time,YawBrMyp,Time,YawBrMzp)
legend('M tilt','M yaw','YawBrMy','YawBrMz')
% xlim([98 100])

figure(3)
plot(Time,detrend(Mf(:,1)),'LineWidth',1), hold on
plot(Time,detrend(Mf(:,2)),'LineWidth',2)
plot(Time,detrend(YawBrMyp),'LineWidth',1)
plot(Time,detrend(YawBrMzp),'LineWidth',2)
legend('M tilt','M yaw','YawBrMy','YawBrMz')
% xlim([98 100])

% The static offset between YawBrMyp and the tilt moment from the MBC is
% because of the static pitch moment caused by rotor overhang

%--------------------------------------------------------------------
% PSD
nfft = length(Time);
fs = 1/(Time(2)-Time(1));
[pRootMyc,~] = pwelch(detrend(RootMyc1,'constant'),[],0,nfft,fs);
[pMf,~] = pwelch(detrend(Mf,'constant'),[],0,nfft,fs);
[pYawBrMyp,~] = pwelch(detrend(YawBrMyp,'constant'),[],0,nfft,fs);
[pYawBrMzp,f] = pwelch(detrend(YawBrMzp,'constant'),[],0,nfft,fs);

figure(4)
loglog(f,pRootMyc)
xline(mean(LSSTipVxa)/60);
title('Blade-root Out-of-plane bending')

figure(5)
subplot(211)
loglog(f,pMf(:,1),'b'), hold on
loglog(f,pYawBrMyp,'r')
```

7.1.2 Code for d&q Transformation:

```
clear
close all
clc
%
% FAST output
FileName = 'D:\Rahul\FAST8\WTM.turb.zerograv.zerotilt.out';
[Channels, ChanName, ChanUnit,DescStr] = ReadFASTtext(FileName);

Time      = Channels(:,strmatch('Time',ChanName));
RootMyc1  = Channels(:,strmatch('RootMyc1',ChanName));
RootMyc2  = Channels(:,strmatch('RootMyc2',ChanName));
RootMyc3  = Channels(:,strmatch('RootMyc3',ChanName));
YawBrMyp  = Channels(:,strmatch('YawBrMyp',ChanName));
YawBrMzp  = Channels(:,strmatch('YawBrMzp',ChanName));
LSSTipPxa = Channels(:,strmatch('LSSTipPxa',ChanName))*pi/180;
LSSTipVxa = Channels(:,strmatch('LSSTipVxa',ChanName));

%
% YawBrMyp0 = -5.255E-04;
% YawBrMyp  = YawBrMyp - YawBrMyp0;

for ii = 1:size(Channels,1)

 %for blade root loads
 a = 2/3*[cos(LSSTipPxa(ii)),cos(LSSTipPxa(ii)+2*pi/3),cos(LSSTipPxa(ii)+4*pi/3);
         cos(LSSTipPxa(ii)),cos(LSSTipPxa(ii)+2*pi/3),cos(LSSTipPxa(ii)+4*pi/3)];
 c = [RootMyc1(ii); RootMyc2(ii); RootMyc3(ii)];

 B(ii,:) = a*c;


 %fixed to rotating
 a2 = [cos(LSSTipPxa(ii)),       sin(LSSTipPxa(ii));
          cos(LSSTipPxa(ii)+2*pi/3),sin(LSSTipPxa(ii)+2*pi/3);
          cos(LSSTipPxa(ii)+4*pi/3),sin(LSSTipPxa(ii)+4*pi/3)];
 c2 = [YawBrMyp(ii);YawBrMzp(ii)];

 B2(:,ii) = a2 * c2;

end


% PSD
nfft = length(Time);
fs = 1/(Time(2)-Time(1));
[pRootMyc,~] = pwelch(detrend(RootMyc1,'constant'),[],0,nfft,fs);
[pRootMyc2,~] = pwelch(detrend(RootMyc2,'constant'),[],0,nfft,fs);
[pRootMyc3,~] = pwelch(detrend(RootMyc3,'constant'),[],0,nfft,fs);
[pB,~] = pwelch(detrend(B,'constant'),[],0,nfft,fs);
```

```
[pB2,~] = pwelch(detrend(B2,'constant'),[],0,nfft,fs);
[pYawBrMyp,~] = pwelch(detrend(YawBrMyp,'constant'),[],0,nfft,fs);
[pYawBrMzp,f] = pwelch(detrend(YawBrMzp,'constant'),[],0,nfft,fs);

figure(4)
loglog(f,pRootMyc),hold on
xline(mean(LSSTipVxa)/60);
title('Blade-root Out-of-plane bending vs d axis transform')

figure(5)
subplot(211)
loglog(f,pB(:,1),'b*'), hold on
loglog(f,pB(:,2),'m'),hold on
loglog(f,pYawBrMyp,'r')
loglog(f,pYawBrMzp,'g')
loglog(f,pRootMyc,'y')
legend('Bdirect BM','BQuad BM','Yaw Bearing Y BM','Yaw Bearing Z BM','Root blade
1 load')

figure(7)
plot(Time,B(:,1),'g*',Time,B(:,2),Time,RootMyc1,Time,YawBrMyp)
legend('Bdirect BM','BQuad BM','Root blade 1 load','Yaw Bearing Y BM')

figure(8)
loglog(f,pRootMyc),hold on
loglog(f,pRootMyc2)
loglog(f,pRootMyc3)
loglog(f,pB2(1,:),'b*')
loglog(f,pB2(2,:),'m')
loglog(f,pB2(3,:),'y*')

figure(9)
loglog(f,pB2(1,:),'b*'),hold on
loglog(f,pB2(2,:),'m')
loglog(f,pB2(3,:),'y*')
loglog(f,pB(:,1))
loglog(f,pB(:,2))
```

7.2 FAST

FAST (Fatigue, Aerodynamics, Structures, and Turbulence) is an aero-servo-elastic-hydro simulation tool designed by the National Renewable Energy Laboratory (NREL) and is publicly available. Each physical domain of the problem, aero-dynamic, elastic and hydrodynamic is assigned to a distinct module. For an onshore wind turbine, four modules are of interest:

1. ElastoDyn [76]: it controls the degrees of freedom that will be active in the simulation, it contains the definition of the turbine geometry, inertia properties and drivetrain. It also includes the structural definition of the blades and the mass, inertia and stiffness distribution. In the FAST model used both for the DTU turbine and for the one in this work, both prebend and precone are neglected, since FAST does not support them now. The turbine motion is split into a rigid and a flexible part, the first being computed by means of a multibody formulation, and the latter based on a modal approach (polynomial mode shapes) that considers up to the first two tower fore-aft and side-side modes, the first edgewise and the first two flap wise modes of the blades. Moreover, FAST can also account for the transmission flexibility and damping by means of a one degree of freedom transmission model between the Low-Speed Shaft (LSS), connected to the rotor, and the High-Speed Shaft (connected to the generator);

2. AeroDyn [46]: this module bears the aerodynamic part of the model; it considers the aerodynamic loads produced by the wind on the turbine. The approach is based on a modified Blade Element Momentum Theory (BEMT). The input for the module includes a set of so-called radial blade stations, in which each blade is supposed to be subdivided into. Each blade station, as for the BEM theory [6] is considered to independently contribute to the overall aerodynamic forces acting on the hub. The software takes in the radial position, width, chord, twist angle, airfoil model and polars for each blade station, and uses them to compute the aerodynamic loads on the blades. AeroDyn is a very powerful tool, that can also account for tip and hub losses, tower shadow, induction factors and dynamic stall. Moreover, the airfoil polars can include stall angle and be Reynolds dependent if the modelist so desires. In conclusion, the module also deals with Inflow Wind (see below) to define the wind field properties around the wind turbine.

3. InflowWind: as mentioned before, this module deals with the definition of the wind field around the wind turbine, it can generate either a smooth, uniform wind field (equal in each point) or account for wind shear and turbulence.

4. ServoDyn: this module manages control operations. The control inputs are three: generator torque, the collective pitch angle for each blade and the nacelle yaw angle. The control logics can be programmed in by the user in Simulink, but FAST also provides built in simplified models for all three inputs.

Bibliography

[1] Offshore Wind Turbine url: https://kth.diva-portal.org/smash/get/diva2:1285492/FULLTEXT01.pdf

[2] Wind Energy data url: https://gwec.net/global-wind-report-2021/

[3] Offshore wind market report 2021 edition url: https://www.energy.gov/sites/default/files/2021-08/Offshore%20Wind%20Market%20Report%202021%20Edition_Final.pdf

[4] Wind Turbine capacity forecast[4] url: https://www.renewableenergyworld.com/wind-power/wind-power-experts-expect-wind-energy-costs-to-decline-up-to-35-by-2035/#gref

[5] M. Bollati, “Aerodynamic and mechanical design of a large-scale rotor wind turbine,” Master’s thesis, Politecnico di Milano, 2017/2018.

[6] M. Usai, “Aerodynamic and mechanical design of an offshore wind turbine prototype,” Master’s thesis, Politecnico di Milano, 2019.

[7] Ilmas Bayati1 , Marco Belloli1 , Luca Bernini1 , Hermes Giberti2 , Alberto Zasso1 “Scale model technology for floating offshore wind turbines” IET Renew. Power Gener., 2017, Vol. 11 Iss. 9, pp. 1120-1126

[8] Semi-Span Test at NTF(NASA Langley Research Center) Keith C. Lynn1 NASA Langley Research Center, Hampton, Virginia, 23681

[9] Two component balance with dimensions : Lincoln P. Erm, http://www.dsto.defence.gov.au/corporate/reports/ DSTO-TR-1835.pdf

]10] Wake measurement of blade in wind tunnel setup, I. Bayati et al. / Energy Procedia 137 (2017) 214–222

[11] Bayati, I., Belloli, M., Bernini, L., Fiore, E., Giberti, H., Zasso, A.. On the functional design of the DTU10 MW wind turbine scale model of LIFES50+ project. Journal of Physics: Conference Series 2016;753(5). doi:10.1088/1742-6596/753/5/052018.

[12] Bayati, I., Belloli, M., Bernini, L., Giberti, H., Zasso, A.. On the scale model technology for floating offshore wind turbines. IET Renewable Power Generation 2017;June. doi:10.1049/iet-rpg.2016.0956.

[13] Bayati, I., Belloli, M., Bernini, L., Zasso, A.. Wind tunnel validation of AeroDyn within LIFES50+ project: Imposed Surge and Pitch tests. Journal of Physics: Conference Series 2016;753(9). doi:10.1088/1742-6596/753/9/092001.

[14] Bak, C.. The dtu 10-mw reference wind turbine. Technical University of Denmark, DTU Wind Energy 2013;

[15] Bayati, I., Belloli, M., Bernini, L., Mikkelsen, R., Zasso, A.. On the aero-elastic design of the DTU 10MW wind turbine blade for the LIFES50+ wind tunnel scale

model. Journal of Physics: Conference Series 2016;753(2). doi:10.1088/1742-6596/753/2/022028.

[16] Bayati, I., Bernini, L., Belloli, M., Zasso, A.. Aerodynamic design methodology for wind tunnel tests of wind turbine rotors. In: Journal of Wind Engineering and Industrial Aerodynamics; vol. June. 2017,doi:10.1016/j.jweia.2017.05.004.

[17] H2020 lifes50+ project. 2016. URL: http://lifes50plus.eu/.

[18] Sauder, T., Chabaud, V., Thys, M., Bachynski, E., Sæther, L.. Real-time hybrid model testing of a braceless semi-submersible wind turbine. Part I: The hybrid approach. In: Proceedings of the International Conference on Offshore Mechanics and Arctic Engineering - OMAE; vol. 6. ISBN 9780791849972; 2016,doi:10.1115/OMAE2016-54435.

[19] Berthelsen, P., Bachynski, E., Karimirad, M., Thys, M.. Real-time hybrid model tests of a braceless semi-submersible wind turbine. Part III: Calibration of a numerical model. In: Proceedings of the International Conference on Offshore Mechanics and Arctic Engineering - OMAE; vol. 6. ISBN 9780791849972; 2016,doi:10.1115/OMAE2016-54640.

[20] Bachynski, E., Thys, M., Sauder, T., Chabaud, V., Sæther, L.. Real-time hybrid model testing of a braceless semi-submersible wind turbine. Part II: Experimental results. In: Proceedings of the International Conference on Offshore Mechanics and Arctic Engineering - OMAE; vol. 6. ISBN 9780791849972; 2016,doi:10.1115/OMAE2016-54437.

[21] Bayati, I., Belloli, M., Ferrari, D., Fossati, F., Giberti, H.. Design of a 6-DoF robotic platform for wind tunnel tests of floating wind turbines. In: Energy Procedia; vol. 53. 2014,doi:10.1016/j.egypro.2014.07.240.

[22] Politecnico di milano. Wind Tunnel. URL: http://www.windtunnel.polimi.it/.

[23] I. Bayati1,M. Belloli1, L. Bernini1, E. Fiore1 H.Giberti2, A.Zasso1 , On the functional design of the DTU10 MW wind turbine scale model of LIFES50+ project: , Journal of Physics: Conference Series 753 (2016) 052018 doi:10.1088/1742-6596/753/5/052018

[24] E. A. Bossanyi*, Garrad Hassan and Partners Ltd, Bristol, UK, Published online 7 July 2005 in Wiley Interscience (www.interscience.wiley.com). DOI: 10.1002/we.166.

[25] Bossanyi E. Individual blade pitch control for load reduction. Wind Energy 2003; 6: 119–128.

[26] Bossanyi EA. Developments in individual blade pitch control. EWEA Special Topic Conference ‘The Science of Making Torque from Wind’, Delft, 2004; 486–497.

[27] Lecture Notes in Wind Engineering, Politecnico di Milano.

[28] Y. Yang, C. Li, W. Zhang, J. Yang, Z. Ye, W. Miao, and K. Ye, “A multi-objective optimization for hawt blades design by considering structural strength,” Journal of Mechanical Science and Technology, 08 2016.

[29] C. L. Bottasso, F. Campagnolo, and A. Croce, “Multidisciplinary constrained optimization of wind turbines,” Multibody System Dynamics, 01 2012.

[30] C. Bak, “3 - aerodynamic design of wind turbine rotors,” in Advances in Wind Turbine Blade Design and Materials (P. Brøndsted and R. P. Nijssen, eds.), Woodhead Publishing Series in Energy, pp. 59 – 108, Woodhead Publishing, 2013.

[31] C. Bak, F. Zahle, R. Bitsche, T. Kim, A. Yde, L. Henriksen, P. Andersen, A. Natarajan, and M. Hansen, “Description of the dtu 10 mw reference wind turbine,” 2013.

[32].Coleman RP, Feingold AM. Theory of Self-Excited Mechanical Oscillations of Helicopter Rotors with Hinged Blades. National Advisory Committee for Aeronautics, (NACA) Report 1351, 1957.

[33]. Vas P. Electrical Machines and Drives: A Space-Vector Theory Approach, Vol. 25. Oxford University Press: USA, 1992.

[34] Bossanyi EA. Individual blade pitch control for load reduction. Wind Energy 2003; 6: 119–128. [Online]. Available: http://onlinelibrary.wiley.com/doi/10.1002/we.76/abstract. (Accessed January 2014).

[35] Van Engelen TG, Van der Hooft EL, Individual pitch control inventory. Technical Report ECN-E-03-138, ECN, Petten, the Netherlands, 2005.

[36] Zhang Y, Chen Z, Cheng M. Proportional resonant individual pitch control for mitigation of wind turbines loads. IET Renewable Power Generation 2013; 7: 191–200. [Online]. Available: http://digital-library.theiet.org/content/journals/ 10.1049/iet-rpg.2012.0282. (Accessed January 2014).

[37] Selvam K, Kanev S, Van Wingerden JW, Van Engelen T, Verhaegen M. Feedback–feedforward individual pitch control for wind turbine load reduction. International Journal of Robust and Nonlinear Control 2009; 19: 72–91. [Online]. Available: http://onlinelibrary.wiley.com/doi/10.1002/rnc.1324/abstract. (Accessed January 2014).

[38] Geyler M, Caselitz P. Robust multivariable pitch control design for load reduction on large wind turbines. Journal of Solar Energy Engineering 2008; 130: 030301–1. [Online]. Available: http://cat.inist.fr/?aModele=afficheN& cpsidt=20604937. (Accessed January 2014).

[39] Bossanyi EA. Further load reductions with individual pitch control. Wind Energy 2005; 8: 481–485. [Online]. Available: http://onlinelibrary.wiley.com/doi/10.1002/we.166/abstract. (Accessed January 2014).

[40] Van Engelen T. Design model and load reduction assessment for multi-rotational mode individual pitch control (higher harmonics control). European Wind Energy Conference, Athens, Greece, 2006; 27–2.

[41] Bossanyi E, Wright A. Field testing of individual pitch control on the NREL cart-2 wind turbine. EWEC2009-European Wind Energy Conference & Exhibition, Marseille, France, 2009.

[42] E. A. Bossanyi∗ Garrad Hassan and Partners Ltd, Silverthorne Lane, Bristol BS2 OQD, UK Copyright © 2002 John Wiley & Sons, Ltd. Wind Energ. 2003; 6:119–128

[43] Ventilated Propeller Blade Loadings and Spindle Moment of a Thruster in Calm Water and Waves. Kourosh Koushan1 , Silas Spence1 , Luca Savio

[44] Analysis of Wind-Turbine Main Bearing Loads Due to Constant Yaw Misalignments over a 20 Years Timespan. Center for Wind Power Drives, RWTH Aachen University, 52062 Aachen, Germany; bjoern.roscher@cwd.rwth-aachen.de (B.R.); Ralf.Schelenz@cwd.rwth-aachen.de (R.S.); georg.jacobs@imse.rwth-aachen.de (G.J.)